The relation between morphology, accretion modes and environmental factors in local radio AGN

M. A. Gendre,[1]⋆ P. N. Best,[2] J. V. Wall[3] and L. M. Ker[2]

[1]*Jodrell Bank Center for Astrophysics, The University of Manchester, Oxford Road, Manchester M13 9PL, UK*
[2]*Institute for Astronomy, Royal Observatory, Blackford Hill, Edinburgh EH9 3HJ, UK*
[3]*Department of Physics and Astronomy, The University of British Colombia, 6224 Agricultural Rd, Vancouver, BC V6T 1Z1, Canada*

ABSTRACT

The goal of this work is to determine the nature of the relation between morphology and accretion mode in radio galaxies, including environmental parameters. The CoNFIG extended catalogue (improved by new K_S-band identifications and estimated redshifts from UKIRT Infrared Deep Sky Survey (UKIDSS), and spectral index measurements from new GMRT observations) is used to select a sub-sample of 206 radio galaxies with $z \leq 0.3$ over a wide range of radio luminosity, which are morphology-classified using the Fanaroff–Riley (FR) classification of extended radio sources. For each galaxy, spectroscopic data are retrieved to determine the high/low excitation status of the source, related to its accretion mode. Environmental factors, such as the host galaxy luminosity and a richness factor, are also computed, generally using the Sloan Digital Sky Survey data. We find the following results: (1) at a given radio luminosity, the FR morphological split of sources is consistent with being the same for both accretion modes. This remains true if analysis is restricted to only rich or only poor environments. If confirmed with a larger sample, this would imply that extended radio morphology is independent of the accretion mode of the black hole, depending only on the power of the resultant jet, and its interactions with the larger-scale environment. (2) Excitation modes seem to be linked to the source environment, with high-excitation galaxies found almost exclusively in low-density environments while low-excitation galaxies occupy a wider range of densities; this result is independent of FR morphology, and is consistent with the different fuelling mechanisms expected for these excitation modes. (3) Independent of excitation mode, FRI sources are found to lie in higher density environments, on average, than FRII sources, consistent with FRI sources having their jets disrupted by a denser surrounding medium. However, there is a significant overlap in environment between the two classes, and no clear driving factor between the FRI and FRII sources is found even when combining radio luminosity, accretion mode, large-scale environment and host galaxy luminosity.

Key words: catalogues – galaxies: active – galaxies: luminosity function, mass function – galaxies: statistics – radio continuum: galaxies.

1 INTRODUCTION

Extended radio-loud active galactic nuclei (AGN) can be classified according to their morphology, following the Fanaroff–Riley (FR) scheme (Fanaroff & Riley 1974), in which FRI objects have the highest surface brightness along the jets near the core, while FRII sources show the highest surface brightness at the lobe extremities, as well as more collimated jets. The division between FRI and FRII is, however, somewhat ambiguous, with the existence of hybrid sources showing jets FRI-like on one side and FRII-like on the other (Capetti, Fanti & Parma 1995; Gopal-Krishna & Wiita 2000).

The FR dichotomy is based purely on the appearance of the radio objects, and the mechanisms differentiating the two populations are still unknown. Two main streams of models have been postulated to explain these differences in morphology. Extrinsic models, purely based on the interaction of the jet with the source environment, were proposed based on environmental differences found between FRI and FRII sources (e.g. Prestage & Peacock 1988), and on their apparently distinct host galaxies (Owen & Ledlow 1994). The hypothesis is that inter-galactic medium (IGM) density is the differentiating factor, where jets of sources in higher/lower density mediums

⋆ E-mail: mgendre@jb.man.ac.uk

experience a higher/lower degree of resistance, yielding sources with FRI/FRII structures, respectively. Intrinsic models, on the other hand, were postulated based on fundamental differences seen between FRI and FRII sources, such as their emission line properties (Zirbel & Baum 1995). These models suggested that the dichotomy arises from differences in the properties of the central black hole (e.g. Baum, Zirbel & O'Dea 1995; Ghisellini & Celotti 2001). In these scenarios, jets produced by low accretion-flow rate which are generally weak, mostly display FRI-type structure, whereas galaxies with higher accretion flow rates give rise to stronger, mainly FRII-type jets.

More recently, these different accretion rates have been associated with the excitation mode of the narrow line region gas in the host galaxy. In low-excitation galaxies (LEG), also known as 'radio-mode' or 'hot-mode' accretors, the accretion on to the black hole is radiatively inefficient but does produce highly energetic radio jets via the emission of kinetic energy through the radio jets (Merloni & Heinz 2007). High-excitation galaxies (HEG), also known as 'quasar-mode' or 'cold-mode' accretors, are linked to radiatively efficient accretion discs (Shakura & Sunyaev 1973) and are often identified with star formation activity in the host galaxies (Kauffmann et al. 2003). Several recent studies (Hardcastle, Evans & Croston 2007; Baldi & Capetti 2008; Kauffmann, Heckman & Best 2008) suggest that HEGs have undergone a recent merger that triggered star formation, driving cold gas towards the central engine, powering the AGN (cold gas accretion). LEGs have had no such recent merger and show no evidence of recent star formation, and are believed to be fuelled by the hot inter-stellar medium (ISM), possibly as part of a feedback cycle (e.g. Best et al. 2005). Thus, although some other alternative explanations for the influx of cold gas in HEGs exists, such as recycled gas from dying stars (Ciotti & Ostriker 2007), mergers or interactions seem to give the most likely explanation for cold gas accretion.

Baldi & Capetti (2008) studied nearby 3CR radio galaxies and their optical properties and found indication of recent star formation in HEGs, but not in the LEGs. In a different study, Emonts et al. (2008) found no evidence for large-scale H I in low-luminosity sources, but significant amounts in high-luminosity sources. The 'radio-mode' accretors were also shown to be fundamentally different from the 'quasar-mode' accretors from X-ray and infrared observation (Hardcastle et al. 2007). Finally, a dedicated study of HEGs and LEGs by Best & Heckman (2012) confirmed that both population have indeed fundamentally different accretion rates (with $L_{HEG} \sim 0.1L_{Edd}$ while $L_{LEG} < 0.01L_{Edd}$) and host galaxy properties (with LEGs being redder and larger and having more massive galaxy and black hole mass than HEGs of similar radio power; see also Janssen et al. 2012).

These distinctions between HEGs and LEGs are very reminiscent of the differences between FRI and FRII sources (e.g. Jackson & Wall 1999). This is because there is a large overlap in populations between FRIs and LEGs, and between FRIIs and HEGs. However, the relation is not one-to-one: small subsets of FRIs are found in HEG samples, as well as many FRIIs being associated with LEGs (e.g. Laing et al. 1994; Willott et al. 2001; Hardcastle et al. 2007; Heywood, Blundell & Rawlings 2007). This implies that the FR dichotomy is not fully dependent on accretion mode.

It has long been known (Longair 1966) that the radio luminosity function undergoes luminosity-dependent evolution, where low-luminosity sources show little or no evolution while high-luminosity sources undergo positive density evolution. In an initial modelling of the space density of radio AGN, Wall & Jackson (1997) and Jackson & Wall (1999) assumed that this was based on a division

of the radio sources into low-luminosity, non-evolving FRIs and high-luminosity, rapidly evolving FRIIs. However, more recent results have shown that, at comparable powers, FRI and FRII sources show strong similarities in evolution (e.g. Snellen & Best 2001; Rigby, Best & Snellen 2008; Gendre, Best & Wall 2010), whereas there are indications from the work of Best & Heckman (2012) that the cosmic evolution of HEGs and LEGs is different at fixed radio luminosity (HEGs show evidence of strong evolution while LEGs are consistent with little evolution). This implies that LEGs and HEGs may be more appropriate as the two fundamental populations of radio-AGN (see also Chiaberge, Capetti & Celotti 2000, 2002; Buttiglione et al. 2010; Herbert et al. 2010; Kunert-Bajraszewskal & Labiano 2010). From there, in the simplest model, the various observable radio morphology must result from external effects, such as ISM/IGM density (FRI versus FRII) and/or jet orientation (compact versus extended).

The goal of this work is to determine the nature of the relation between morphology and accretion mode in radio galaxies, including environmental parameters. It is based on the extended CoNFIG catalogue (Gendre & Wall 2008; Gendre et al. 2010), which has been improved in terms of spectral index and redshift using both new GMRT radio observations and literature data (Section 2). From there, a comparative study of the FRI/II in the Local Universe ($z \leq 0.3$) is performed, particularly looking into the FR morphology–accretion mode connection, including environmental parameters. For this purpose, excitation classifications, host galaxy luminosity and cluster richness measurements [from the Sloan Digital Sky Survey (SDSS; York et al. 2000), the SuperCosmos Sky Survey (SSS; Hambly et al. 2001), and the ESO Imaging Survey (EIS; Nonino et al. 1999)] were introduced to the local CoNFIG sub-sample (Section 3). The results are then discussed in Section 4.

Throughout this paper, we assume a standard Λcold dark matter cosmology with $H_0 = 70 \, \text{km s}^{-1} \, \text{Mpc}^{-1}$, $\Omega_M = 0.3$ and $\Omega_\Lambda = 0.7$.

2 IMPROVING THE CONFIG SAMPLE

The extended CoNFIG catalogue (Gendre et al. 2010) is a sample of radio sources at 1.4-GHz, combining seven samples [3CRR, Laing, Riley & Longair 1983; CoNFIG1-4, Gendre & Wall 2008; Combined EIS-NVSS Survey Of Radio Sources (CENSORS), Best et al. 2003; and Lynx & Hercules, Rigby, Snellen & Best 2007] covering a large range of flux densities (from $S_{1.4 \, \text{GHz}} \geq 0.5 \, \text{mJy}$ for Lynx & Hercules to $S_{1.4 \, \text{GHz}} \geq 3.5 \, \text{Jy}$ for 3CRR). It includes FRI/FRII/Compact morphology classifications, optical identifications and redshift estimates. It contains 1114 sources and is 94.3 per cent complete for radio morphological classifications. Improvements to the catalogue are described in the following sections.

2.1 GMRT data

In order to complete the spectral index coverage of the CoNFIG1-4 samples, GMRT data were obtained on 2011 July 4 for 48 sources. They were observed over 9 h in total (5 to 30 min on target depending on the source), with a central frequency of 591-MHz and a 33.3-MHz bandwidth divided into 256 channels. The source 3C 147 was used to calibrate flux densities and the data were reduced using standard AIPS procedures so as to reach an rms noise of $\sigma \approx 0.5 \, \text{mJy bm}^{-1}$.

Flux densities were measured for all sources (Table A1), and the FRI/FRII morphology was confirmed for four sources with previously 'possible' classification (Gendre et al. 2010): 4C 04.41 (C1-128, FRI), 4C 03.27 (C1-163, FRI), 4C 16.30 (C2-095, FRII)
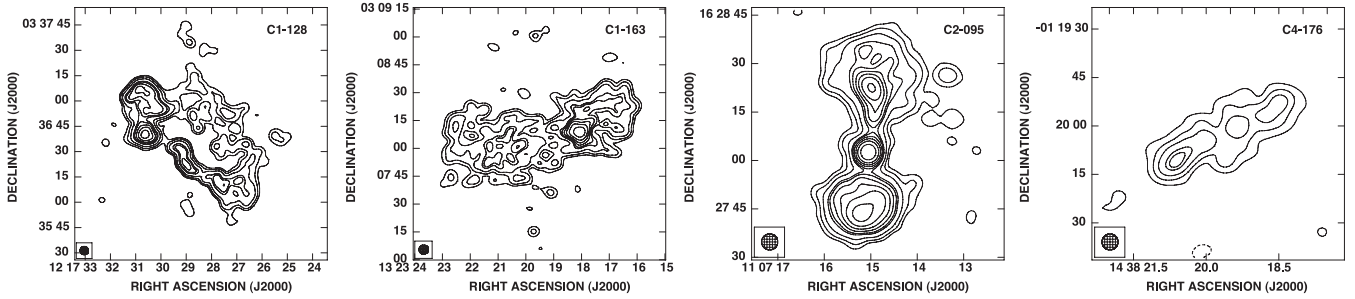
Figure 1. GMRT 591-MHz continuum observation contour maps at $-1, 1, 2, 4, 8, 10, 14, 20, 30, 50 \times 1.5$ mJy bm^{-1} for the sources (from left to right) 4C 04.41, 4C 03.27, 4C 16.30 and 1438−0133. The reference catalogue number for each source is shown on the top-right corner of each image.

and 1438−0133 (C4-176, FRII). Contour plots for these sources are shown in Fig. 1.

2.2 Spectral index

Using the GMRT flux density measurements described in the previous section, in combination with the 1.4-GHz flux density data, previously unavailable spectral index values were computed for 46 sources. Spectral index determinations were also improved for a further 91 CoNFIG sources by including flux-density information from the VLA Low-frequency Sky Survey at 74 MHz (VLSS; Cohen et al. 2007) and from the Cosmic Lens All Sky Survey of radio sources at 8.4 GHz (CLASS; Myers et al. 2003), or by recording values previously published. As specified by Gendre et al. (2010), low-frequency spectral index determinations are preferred for our analysis, but high-frequency indices were used whenever the low-frequency ones were unavailable.

The revised and new spectral index values are presented in Table A2.

2.3 *K*-band magnitude and redshifts

Additional host-galaxy cross-identifications were performed using the UKIRT Infrared Deep Sky Survey DR9 (UKIDSS; Lawrence et al. 2007). UKIDSS uses the UKIRT Wide Field Camera (WF-CAM; Casali et al. 2007) and a photometric system described in Hewett et al. (2006). The pipeline processing and science archive are described in Hambly et al. (2008).

After visual inspection, *K*-band magnitudes (through a 2.0 arcsec aperture diameter) were retrieved for 190 CoNFIG sources (Table A3), including 20 new identifications (Table A4) and 48 extended radio sources with known spectroscopic redshifts. We computed a *K*–*z* relation appropriate to their magnitude determination [$\log(z) = 0.305K$-5.319], which is in line with other *K*–*z* relations (e.g. Willott et al. 2001; Brookes et al. 2006), and got the first redshift estimates for 25 FRI/II sources (including sources with optical identification but no previously available photometric or *K*–*z* redshift estimates). In addition, publications of new or updated catalogues (e.g. Croom et al. 2009; Richards et al. 2009) also allowed us to improve the redshift coverage of sources in the extended CoNFIG catalogue. The new redshift values are shown in Table A5. Finally, redshift and spectral index information were updated for the CENSORS sample (Brookes et al. 2006) according to the work of Ker et al. (2012).

The improved catalogue includes a total of 760 extended sources (131 FRIs, 566 FRIIs and 63 uncertain) and 336 compact sources (not including 18 CSS sources), with 93.3 per cent spectral index completion (99.3 per cent for the four CoNFIG samples) and

82.9 per cent (spectroscopic or photometric) redshift coverage, making it one of the largest, most comprehensive data bases of morphologically classified radio sources and an important tool in the study of AGN space densities.

2.4 The CoNFIG local sub-sample

To investigate the nature of the physical processes behind the FR dichotomy, its relation to high/low excitation classification, and its dependence on environmental richness factor and host-galaxy luminosity, a sub-sample of local ($z \leq 0.3$) CoNFIG extended radio sources was compiled. The sub-sample contains 206 sources, comprising 73 FRIs, 103 FRIIs, five unclassified extended and 25 compact objects, and it is 99.5 per cent complete for spectral index and optical identification.

3 THE FR DICHOTOMY IN THE LOCAL UNIVERSE

3.1 FRI/FRII LRLFs

Using the updated extended CoNFIG catalogue, the local radio luminosity functions (LRLF) were computed using the $1/V_{max}$ technique for $z \leq 0.3$ (with $\log P_{1.4\,GHz} \geq 22.0$ W Hz^{-1} sr^{-1}), in which, for each *P*–*z* bin, the space density is given by

$$\rho = \sum_{i=1}^{N} \frac{1}{V_i} \qquad \sigma^2 = \sum_{i=1}^{N} \frac{1}{V_i^2} \tag{1}$$

where V_i is the largest volume in which the source could be observed in bin *i*.

Comparing the FR LRLFs presented here (Fig. 2 and Table 1) with fig. 12 of Gendre et al. (2010), the improvement in CoNFIG allowed for a better definition of the LRLFs. In particular, for FRIs, the space density determinations extend to higher luminosities, while at lower luminosities, the FRII LRLF seems to plateau for $\log P_{1.4\,GHz} \leq 23.8$ W Hz^{-1} sr^{-1}.

3.2 High/low excitation galaxies

In this work, HEG/LEG classification was determined by measuring the [O III] ($\lambda_{[O III]} = 5007$ Å) and [O II] ($\lambda_{[O II]} = 3727$ Å) lines, and following the definitions of Jackson & Rawlings (1997): sources with rest-frame [O III] equivalent width (EW) < 1 nm and/or [O II]/[O III] > 1 were classified as LEG, other sources being classified as HEG. If no [O III] line was detected in the spectrum (in which an EW $\sim$ 1 nm line would be otherwise detected), the source was considered to be low excitation.
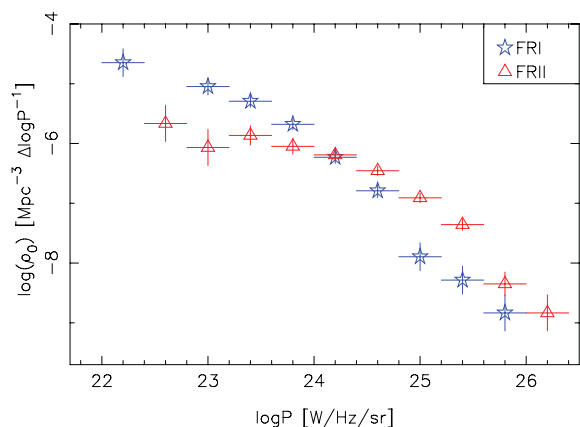
Figure 2. Updated local radio luminosity function $\rho(P)$ for FRIs and FRIIs, using bin sizes of $\Delta \log P_{1.4\,\mathrm{GHz}} = 0.4$, represented by stars and triangles, respectively.

Table 1. Local luminosity functions $\rho(P)$ data from Fig. 2 – FRI/FRII LRLF – and Fig. 3 – HEG/LEG LRLF. P corresponds to the central 1.4 GHz luminosity of the bin (with $\Delta \log P_{1.4\,\mathrm{GHz}}=0.4$), and is given in W Hz^{-1} sr^{-1}. Space densities are in Mpc$^{-3}\Delta \log P_{1.4\,\mathrm{GHz}}^{-1}$.

P	$\log_{10}(\rho)$			
	FRI	FRII	LEG	HEG
22.2	-4.66 ± 0.23	–	-5.21 ± 0.30	–
22.6	–	-4.65 ± 0.23	–	-5.67 ± 0.30
23.0	-5.06 ± 0.14	-5.05 ± 0.14	-5.19 ± 0.16	–
23.4	-5.29 ± 0.10	-5.29 ± 0.10	-5.25 ± 0.24	–
23.8	-5.69 ± 0.09	-5.68 ± 0.09	-5.53 ± 0.17	-6.33 ± 0.52
24.2	-6.23 ± 0.10	-6.23 ± 0.10	-6.04 ± 0.23	-6.64 ± 0.59
24.6	-6.79 ± 0.11	-6.79 ± 0.11	-6.68 ± 0.43	-6.51 ± 0.31
25.0	-7.89 ± 0.23	-7.89 ± 0.23	-7.47 ± 0.63	-7.06 ± 0.32
25.4	-8.28 ± 0.23	-8.28 ± 0.23	-7.92 ± 0.65	-7.41 ± 0.29
25.8	-8.83 ± 0.30	-8.83 ± 0.30	-8.36 ± 0.20	-7.99 ± 0.14
26.2	–	-8.83 ± 0.30	–	–

For the CoNFIG local sub-sample, we found 88 LEGs (including 49 FRIs and 29 FRIIs) and 70 HEGs (including 11 FRIs and 47 FRIIs). The 48 other sources (including 13 FRIs and 27 FRIIs) did not have spectra available to determine the excitation level of the host galaxy. The HEG/LEG classification is shown in Table B1.

Looking at the host galaxy properties of sources with no HEG/LEG classification available, no major systematic offsets in magnitude or other properties were observed compared to other radio sources of the same redshifts and radio fluxes. The local radio luminosity function was computed for both HEGs and LEGs following equation (1), with these unclassified sources were therefore considered to be a random sub-sample and were taken into account by correcting each luminosity bins of the LRLFs by a factor:

$$F = 1 + \frac{\sum_{i=1}^{N} \frac{1}{V_i}\Big|_{\mathrm{unclass}}}{\sum_{i=1}^{N} \frac{1}{V_i}\Big|_{\mathrm{classified}}}. \quad (2)$$

The resulting LRLFs are shown in Fig. 3. We see that for both HEGs and LEGs, the data cover the full range of radio luminosities studied ($22.0 \leq \log P_{1.4\,\mathrm{GHz}} \leq 26.0$ W Hz^{-1} sr^{-1}), and they agree well with the work of Best & Heckman (2012), indicating that the inclusion of sources with no HEG/LEG classification was properly done. Indeed, in regions of the LRLF where the space density of HEGs and LEGs differs by an order of magnitude, if too many
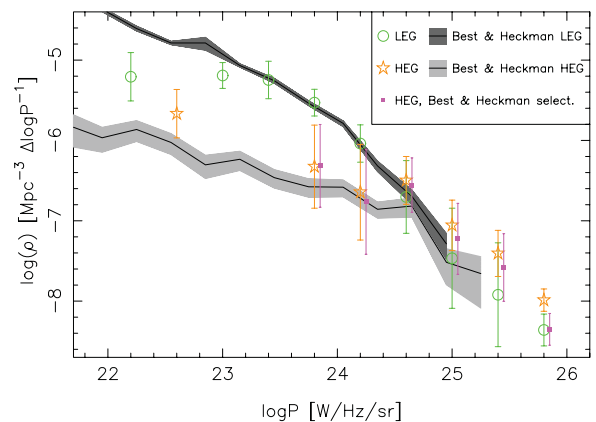
Figure 3. Local radio luminosity function $\rho(P)$ for HEGs (stars) and LEGs (circles) separately, using bin sizes of $\Delta \log P_{1.4\,\mathrm{GHz}} = 0.4$. The LRLFs are compared to results from Best & Heckman (2012) (in light and dark grey for HEGs and LEGs, respectively). For more accurate comparisons, the LRLF for CoNFIG HEGs with SDSS counterparts (excluding quasars) as selected by Best & Heckman (2012) is shown in filled squares.

unclassified sources had been added to the less-dominant population, they could have produced a factor of a few increase on that LRLF. We do find a higher space density of HEGs in our sample for $\log P_{1.4\,\mathrm{GHz}} \geq 24$ W Hz^{-1} sr^{-1} relative to Best & Heckman (2012), but no deficiency in LEGs. Part of this is caused by Best & Heckman's exclusion of quasars which, although a small proportion of the overall sample, are a significant fraction of high power HEGs. Nevertheless, a small excess is still present when applying the Best & Heckman (2012) selection criteria, suggesting that optically selected samples, such as SDSS, might be under-sampling high-power HEGs.

3.3 Cluster richness

Cluster richness for each source was determined using the method of Wing & Blanton (2011), in which the richness factor N_1^{-19} corresponds to the corrected number of SDSS galaxies with absolute magnitudes brighter than $M_r = -19$ within a 1.0 Mpc radius of the radio source. The corrected galaxy count is obtained by measuring the total number of sources in the 1.0 Mpc-radius disc and subtracting a background count, measured from a shell of inner and outer radii 2.7 and 3.0 Mpc, respectively.

When SDSS data were unavailable (20.4 per cent of the local sample), SuperCosmos Sky survey R-band (28 sources) and EIS Patch-D I-band (14 CENSORS sources) data were used. The r-band to R-band and r-band to I-band magnitude limit conversion were determined from sources in the CoNFIG local sample with both data available, and are given as

$$R = r - 0.64 \ (\sigma_{\mathrm{rms}} = 0.09) \quad (3)$$

$$I = (r - 0.46) - 0.75 \ (\sigma_{\mathrm{rms}} = 0.3) \quad (4)$$

with $I = i - 0.75$ as the standard conversion from Windhorst et al. (1991).

According to Wing & Blanton (2011), a cluster-richness of $N_1^{-19} \leq 20$ likely corresponds to a poor environment, while $N_1^{-19} \geq 40$ corresponds to a rich cluster. It was thus decided to use $N_1^{-19} = 30$ to differentiate between poor and rich environments.

Values of N_1^{-19} for sources in the local CoNFIG sub-sample are shown in Table B1.

4 RESULTS AND DISCUSSION

4.1 HEG/LEG

The possibility that FR types depend on the distinct accretion mode inside the central SMBH is examined by looking at the probability of a HEG/LEG being of a given FR type.

The fractions of HEG and LEG being FRII, as a function of radio power, are displayed in the left panel of Fig. 4. The two distribution overlap within the errors, which include both uncertainty due to sources with no HEG/LEG classification (17.6 per cent of FRI and 26.5 per cent of FRIIs) and Poisson statistics dependent on the number of sources in each luminosity bin considered. It appears that Poisson errors are the main source of uncertainty here.

A Pearson chi-square test, including Yate's correction when appropriate, was performed on the FRI/FRII HEG/LEG samples for each luminosity bin (right panel of Fig. 4). The degree of uncertainty imposed by the lack of complete classification is indicated here by including sources with no excitation classification in different categories and is represented as error bars. In most luminosity bins (apart from $23.95 \leq \log P_{1.4\,\mathrm{GHz}} \leq 24.55\,\mathrm{W\,Hz^{-1}\,sr^{-1}}$), the probability of radio morphology being independent of excitation is greater than 5 per cent, and up to $P_{\mathrm{FR\text{-}H/L}} > 80$ per cent in a third of cases. For the intermediate luminosity range singled out above, there is some indication that there might be a difference at the 5 per cent confidence limit. However, the idea that there is a dependence on excitation state at intermediate luminosities that is not present at other luminosities seems unphysical, in particular when considering the relatively low confidence level of the difference. Especially, when considering the potential influence of sources without excita-

tion classification, it appears possible that FRI/FRII is independent of HEG/LEG type over the whole range of luminosity considered.

Thus, based on the above results, the null hypothesis that, at given radio luminosity, FR morphology is independent of the accretion-mode of the black hole cannot be ruled out.

4.2 Environmental influences

4.2.1 Cluster richness

The idea that, no matter how they are produced, jets will behave differently depending on the cluster environment they encounter is a possible explanation for the different FR morphologies, independently of excitation types. Environmental statistics for each of the populations considered in this work are presented in Table 2, while Fig. 5 shows the distribution of richness factor with respect to radio powers. Note that, based on Fig. 5, it seems that radio power offsets

Table 2. Environmental parameters for each of the populations (FRI, FRII, HEG, LEG and combinations) considered in this work.

Type	Number of sources			Richness	
	Total	Poor	Rich	Mean $(\mu \pm \Delta\mu)$	Median M
FRI	73	36	37	31.9 ± 7.7	29.8
FRII	103	77	26	20.3 ± 3.4	14.9
HEG	58	56	14	19.8 ± 5.3	15.1
LEG	78	48	40	31.9 ± 7.1	29.8
Unk.	40	35	13	19.6 ± 4.4	15.7
FRI-HEG	11	9	2	14.3 ± 10.3	3.6
FRI-LEG	49	21	28	36.3 ± 11.0	35.8
FRII-HEG	47	38	9	21.0 ± 6.1	15.4
FRII-LEG	29	18	11	24.6 ± 4.5	14.3
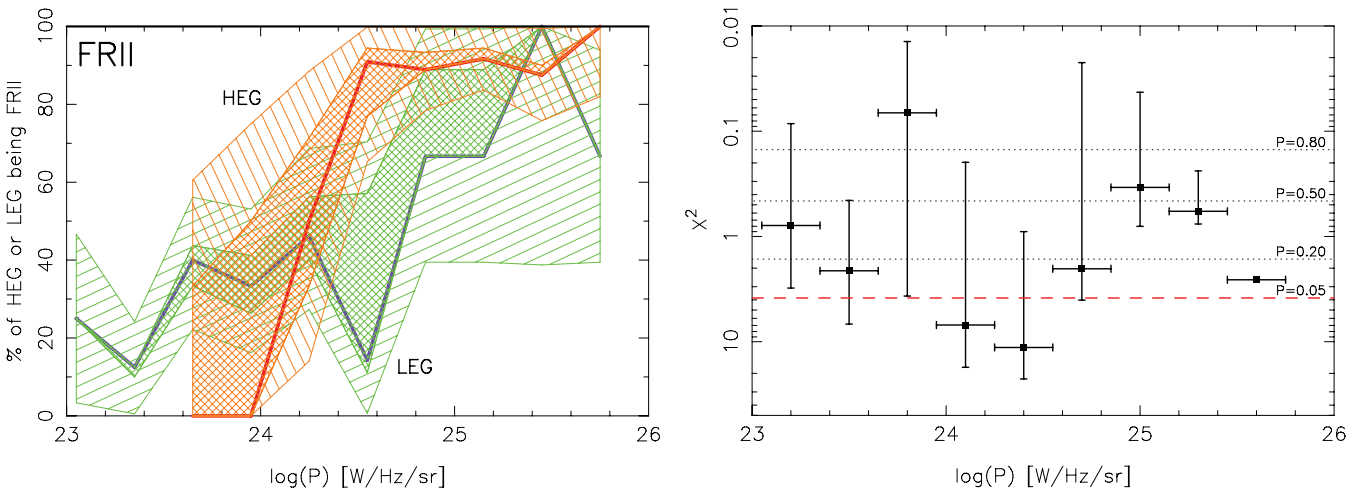
Figure 4. Left: percentage of HEGs (thick red line) and LEGs (thick purple line) being FRII in the CoNFIG local sub-sample (excluding sources with no HEG/LEG classification). The luminosity bins are $\Delta \log P = 0.3$ wide. The cross-hatched regions correspond to the minimum and maximum possible values of the ratios when including sources with unidentified spectral type, and the hatched regions include errors in these limits depending on the number of sources in each bin following Poisson statistics. Right: result of the Pearson chi-square test performed on the FRI/FRII HEG/LEG samples for each luminosity bin. For comparison, χ^2 values corresponding to a probability $P = 0.2$, 0.5 and 0.8 that radio morphology is independent of excitation are displayed in dotted lines. The dashed line represents the value of χ^2 for which $P = 0.05$, the lowest acceptable probability for which the distributions are independent accepted here. For each luminosity bin, the range of possible χ^2 values when including unclassified sources is determined based on the minimum and maximum values of χ^2 in each of the following extreme cases: (i) no unclassified sources are taken into account; (ii) all unclassified sources are LEG; (iii) all unclassified sources are HEG; (iv) all FRI unclassified sources are LEG while all FRII unclassified sources are HEG; (v) all FRI unclassified sources are HEG while all FRII unclassified sources are LEG. These error bars indicate the degree of uncertainty imposed by the lack of complete classification.
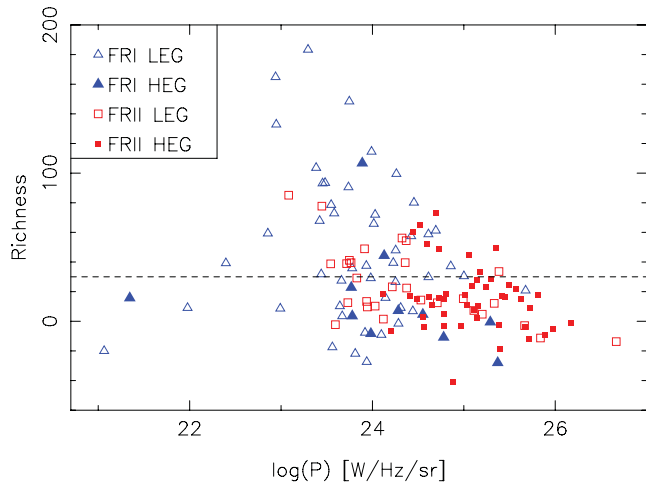
Figure 5. Richness factor as a function of radio power for FRI (blue triangles) and FRII (red squares) HEGs (filled symbols) and LEGs (open symbols). The dashed line corresponds to $N_1^{-19} = 30$, the limit between poor and rich cluster as defined in Section 3.3.

between FRI and FRII sources will not be a strong source of bias in the following analysis.

Looking at the environmental difference between FRI and FRII only, a Pearson chi-square test leads to $\chi^2_{\nu=1} = 9.07$, rejecting the

hypothesis that FR morphology and environment parameters are independent with probability $P_{FR} = 0.990$. With median richness $M_I = 29.8$ and $M_{II} = 14.9$, it appears that FRI sources tend to be located in richer clusters than FRIIs, as previously stated by Zirbel (1997) and Prestage & Peacock (1988).

Focusing on environmental differences between HEGs and LEGs, it can be seen in Fig. 5 that HEGs are found almost exclusively in low-density environments, with median richness $M_H = 15.1$. In contrast, LEGs are found in a wider range of densities. A Pearson chi-square test is performed on samples of HEGs and LEGs in poor and rich clusters (ignoring unclassified sources) leading to $\chi^2_{\nu=1} = 14.23$, rejecting the hypothesis that excitation mode and environment parameters are independent with probability $P_{H/L-Rich} = 0.998$. The dependence of the accretion mode on the environment can possibly be explained by the feeding mechanism associated with each type. Indeed, these results are consistent with HEGs being the result of interactions or mergers (which tend to occur in groups, with lower densities than clusters), while the gas supply of LEGs originates from the cooling out of either the host galaxy itself (possible in both rich and poor environments) or the cluster halo (requiring high densities).

Since both FRI/FRII and HEG/LEG sources show significant environmental influence, and since there are large overlaps in FRI-HEG and FRII-LEG populations, it is essential to test whether both of these relations are independently valid, or whether one is being driven by the other. The richness distribution of FRI/FRII HEGs/LEGs is shown in Fig. 6.
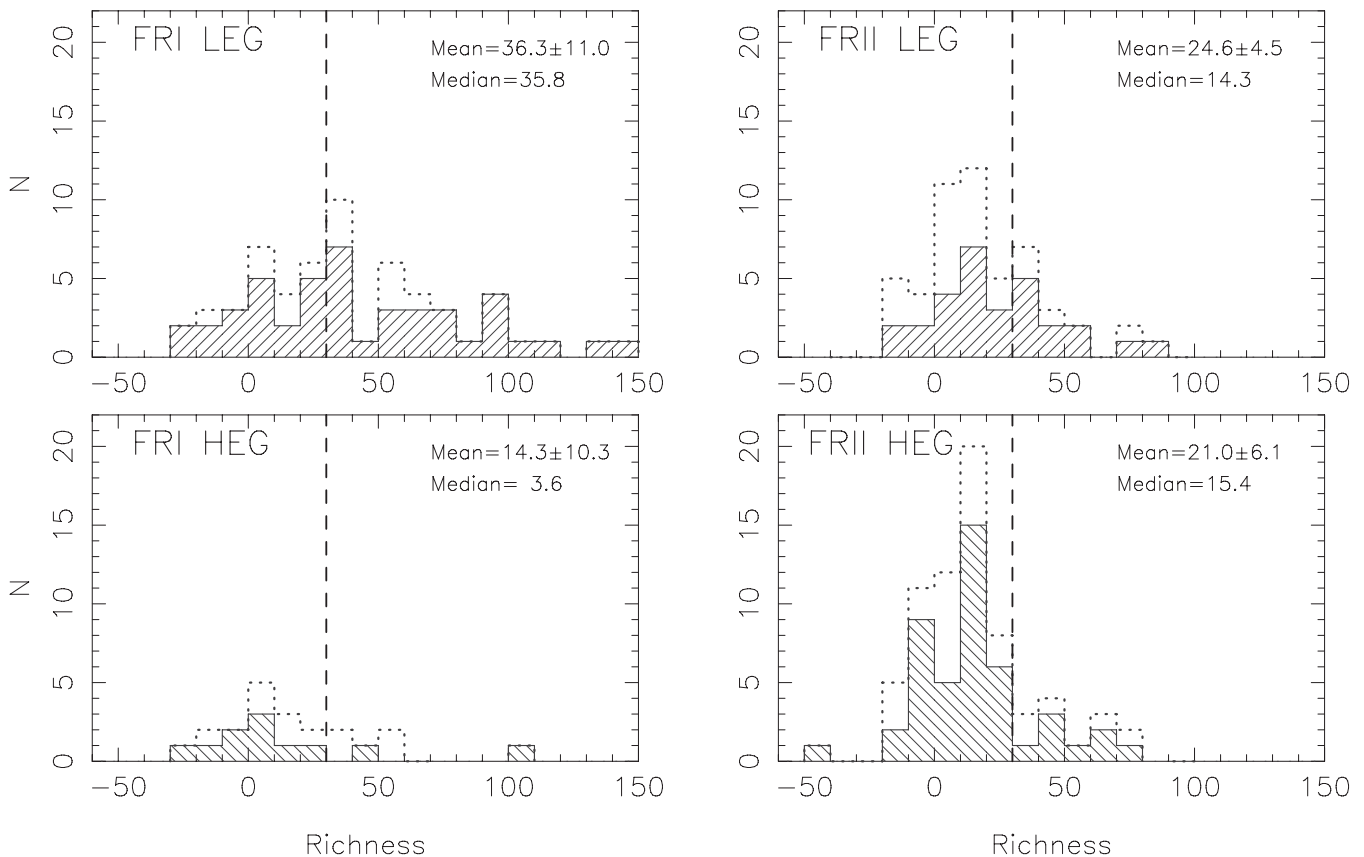
Figure 6. Richness distribution for FRI (left) and FRII (right) LEG (top) and HEG (bottom) sources in the CoNFIG local sub-sample. The dashed line corresponds to $N_1^{-19} = 30$, the limit between poor and rich cluster as defined in Section 3.3. The richness distribution taking into account sources for which HEG/LEG classification was not possible is represented as dotted histograms. Mean, error on mean and median richness (without unclassified sources) are quoted for each distribution.

To further look into a possible FR morphology–excitation mode dependence (or lack thereof), a Kolmogorov–Smirnov test is performed for four comparative cases: FRI HEGs and LEGs, FRII HEGs and LEGs, LEG FRIs and FRIIs and HEG FRIs and FRIIs. The probabilities that the considered samples are drawn from the same distribution are $P_{I–H/L} = 0.02$, $P_{II–H/L} = 0.30$, $P_{L-I/II} = 0.02$ and $P_{H-I/II} = 0.27$, respectively. The probability $P_{I–H/L}$ seems to indicate that, for FRI sources, HEGs and LEGs show a difference in richness. There is hence an environmental dependence on HEG/LEG not driven by FR morphology. Similarly, the low value of $P_{L-I/II}$ shows that there exists an environmental dependence on FRIs/FRIIs not driven only by the accretion mode of the source. Overall, FRI–LEGs stand out as the only class with a substantial number of sources located in high-density environments. When restricting the test to a narrow luminosity range ($23.5 \leq \log P_{1.4\,GHz} \leq 25.0\,W\,Hz^{-1}\,sr^{-1}$), thus reducing as much as possible the effects of any trends with luminosity, similar results ($P_{I–H/L} = 0.01$, $P_{II–H/L} = 0.97$, $P_{L-I/II} = 0.02$ and $P_{H-I/II} = 0.32$) were found, verifying that no biases are caused by underlying correlation between luminosity and environment.

Finally, a similar analysis to the one presented in Section 4.1 is performed, looking at the fractions of HEG and LEG being FRII in poor ($N_1^{-19} \leq 30$) and rich ($N_1^{-19} > 30$) environments (top panels of Fig. 7). A Pearson chi-square test, including Yate's correction

when appropriate, was performed in each case (bottom panels of Fig. 7). For poor clusters, the probability of radio morphology being independent of excitation is greater than 5 per cent for most luminosity bins, even when including sources with no excitation classification. The results are similar for sources in rich clusters. Overall, this suggests that radio morphology is not fully determined by the combination of accretion mode and cluster density.

4.2.2 Host galaxy

According to the previous results, the disruption of the jets leading to the different FR types, although having some dependence on large cluster scale, still shows a clear overlap of environment densities. Another factor considered in this work is that the disruption occurs on the scale of the host galaxy. This was suggested by Ledlow & Owen (1996), who found that the FR division is a function of both optical and radio luminosity while considering sources in the 3CR sample. However, several recent studies (Best 2009; Wing & Blanton 2011), based on other independent samples, failed to replicate the sharp division found between FR populations, finding a large overlap around the Ledlow–Owen divide. Looking at the $M_I - \log P_{1.4\,GHz}$ plots for the CoNFIG local sub-sample presented in Fig. 8, it is apparent that the result of Ledlow–Owen (1996) does
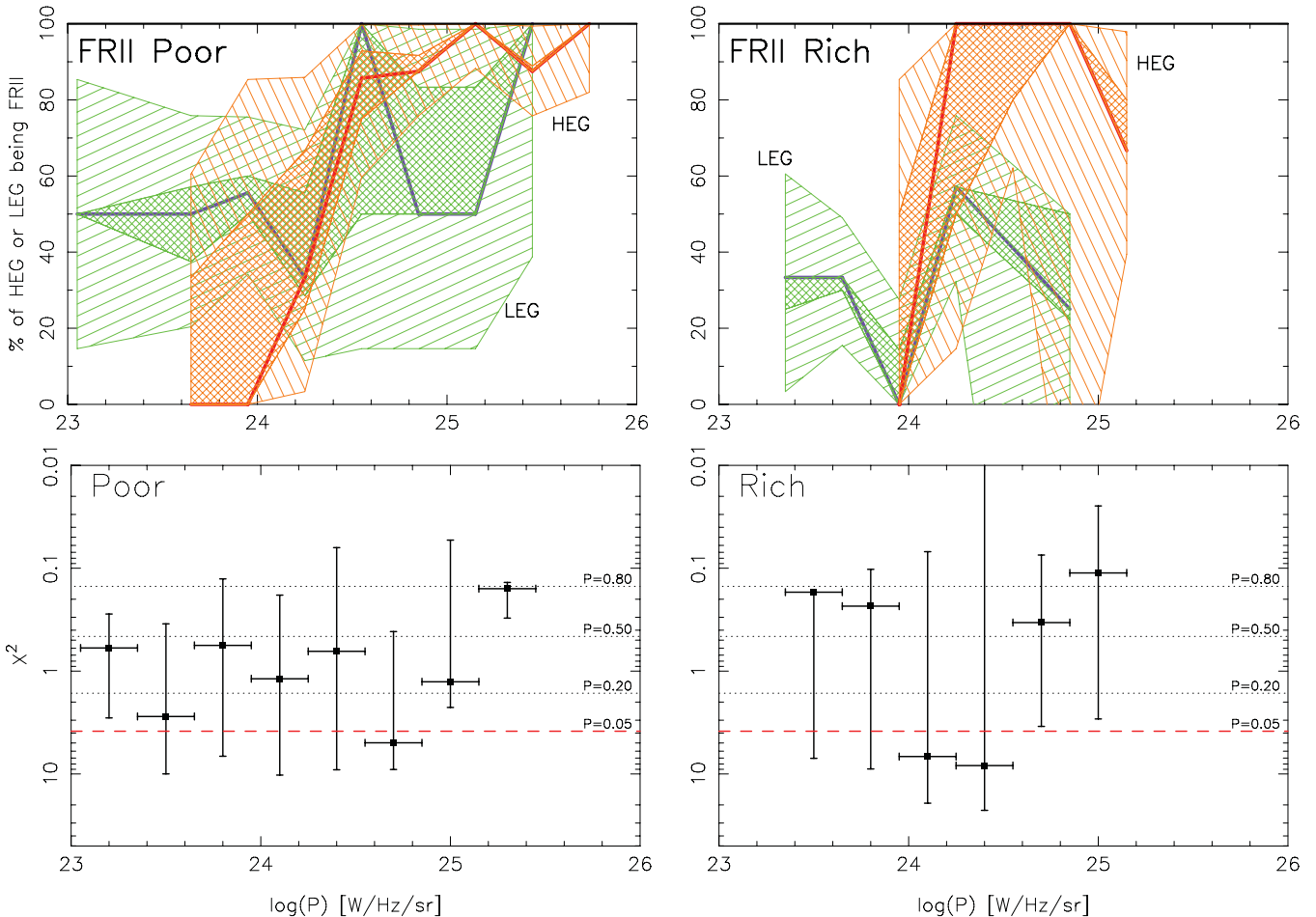
Figure 7. Top: percentage of HEGs and LEGs being FRII in a poor (left) or rich (right) cluster in the CoNFIG local sub-sample (excluding source with no HEG/LEG classification), with identical references as Fig. 4. The last point of the rich LEG ratios was computed in a bin of size $\Delta \log P = 0.9$ to increase the number of sources in the bin. Bottom: result of the Pearson chi-square test performed on the FRI/FRII HEG/LEG samples for each luminosity bin in a poor (left) or rich (right) cluster, with identical references as Fig. 4.
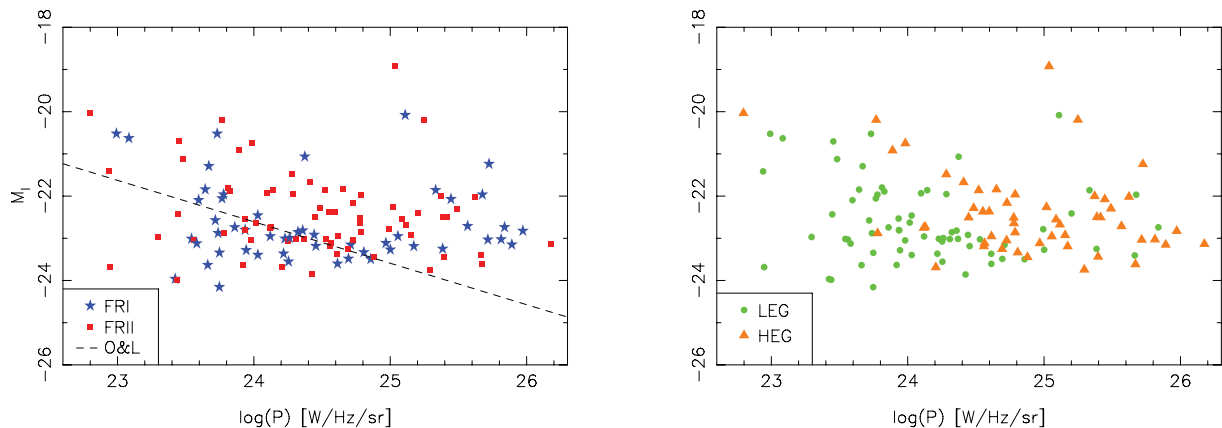
Figure 8. Optical *I*-band versus radio luminosity for FRI and FRII (left panel) and LEGs and HEGs (right panel), excluding quasar sources. For the FRI/II plot, the Ledlow & Owen (1996) relation is also displayed.

not hold for the CoNFIG local sub-sample, even when considering the different intrinsic and extrinsic parameters. This implies that radio galaxies of different FR type are not hosted by significantly different galaxies. In contrast, HEGs and LEGs appear to occupy different regions of the $M_I - \log P_{1.4\,\mathrm{GHz}}$ space. However, this separation is mostly radio-power driven. Note that in the luminosity range $24.0 \leq \log P_{1.4\,\mathrm{GHz}} \leq 25.0\,\mathrm{W\,Hz^{-1}\,sr^{-1}}$, the transition luminosity ranges between the HEG/LEG and FRI/FRII luminosity functions, some trends can be observed, such as FRII being hosted by galaxies extending to lower optical luminosity than FRIs at a given radio power. The significance of these trends is weak, and they are not present at other radio luminosities, but it is notable that this is the same radio luminosity range in which a potential difference was also observed in Fig. 4. A larger sample will be required to establish whether these differences are real.

5 DISCUSSION AND CONCLUSION

In this paper, a sub-sample of local ($z \leq 0.3$) sources from the extended CoNFIG catalogue was used to determine the nature of the relation between morphology and accretion mode in radio galaxies, including environmental parameters. High/low-excitation status were determined for each source by retrieving spectroscopic data, in the majority from SDSS, and comparing the characteristics of [O II] and [O III] lines. Cluster richness factors were computed for each source based on the method presented in Wing & Blanton (2011), from SDSS, SSS or EIS photometric data. The local sub-sample contains 206 sources, including 74 FRIs and 102 FRIIs and is 100 per cent and 76.7 per cent complete for cluster density and HEG/LEG classification, respectively.

Based on this combined knowledge of a source's optical and radio luminosities, environment and excitation mode, the results are as follows.

(i) At a given radio luminosity, both accretion modes show similar FR morphological split of sources, overall as well as when restricting the analysis to only rich or only poor environments. This could imply that extended radio morphology is depending only on the power of the resultant jet, and its interactions with the larger-scale environment, and not on the accretion mode of the black hole.

(ii) HEG are found almost exclusively in low-density environments while LEGs occupy a wider range of densities, independent of FR morphology. This is consistent with the different fuelling mechanisms expected for these excitation modes.

(iii) It appears that radio sources in rich clusters have a higher probability of being FRI and show low-excitation. This can be explained by the fact that jets in massive galaxies with low cooling-rates, giving rise to LEGs (Hardcastle et al. 2007), are easily disrupted, resulting in FRI-like morphologies in dense environments. On the other hand, a HEG/LEG in a poor/rich environment has roughly equal probabilities of being of morphological type-I or type-II, within errors. However, there is a significant overlap in environment between the two classes, and no clear driving factor between the FRI and FRII sources is found even when combining radio luminosity, accretion mode, large-scale environment and host galaxy luminosity.

(iv) The Ledlow & Owen (1996) relation does not hold for the CoNFIG local sub-sample, even when considering the different intrinsic and extrinsic parameters.

The results of this study hint towards the fact that, although originating from two different production mechanisms, the jets of FRI and FRII sources appear to be effectively the same, and to not behave differently in distinct environments. These conclusions are, however, highly dependent on the errors associated with the samples, in particular on the completeness of HEG/LEG classification (when including these sources based on the idea that they are a random subset of HEGs and LEGs, the Poisson errors become 20 per cent smaller). Yet, this result is supported by the fact that radio galaxies of different FR type are not hosted by significantly different galaxies, whereas HEGs and LEGs are.

If intrinsic and large-scale environmental parameters do indeed fail to fully explain the morphological differences between radio sources, it is possible that the distinction FRI/FRII is based on small-scales characteristics, such as the gas mass in the host galaxy (independent of the host mass). This connection between radio morphology and gas mass in the most powerful AGNs in the Local Universe has been previously explored by Evans et al. (2005) and Ocaña Flaquer et al. (2010). They found that molecular gas mass in FRII is a factor of ∼4 greater than in FRI. However, as stated by Ocaña Flaquer et al. (2010), this might be a result of Malmquist bias, with the FRII sources that they study being systematically at higher redshift (and thus showing greater powers) than FRIs. In addition, their samples contained a nearly one-to-one correspondence between FRI and LEG, and between FRII and HEG, meaning that their results could entirely be driven by an underlying LEG/HEG difference in molecular gas properties (as has been established by Smolčić & Riechers (2012). To separate out the effects of HEG/LEG

and FR differences, and hence understand the causes of jet disruption differences in FRIs and FRIIs, it is essential to investigate cross-populations (FRI HEGs and FRII LEGs), for example using high-resolution ALMA sub-mm observations of sources in the CoNFIG local sub-sample.

REFERENCES

Baldi R. D., Capetti A., 2008, A&A, 489, 989
Baum S. A., Zirbel E. L., O'Dea C. P., 1995, ApJ, 451, 88
Best P. N., 2009, Astron. Nachr., 330, 184
Best P. N., Heckman T. M., 2012, MNRAS, 421, 1569
Best P. N., Arts J. N., Röttgering H. J. A., Rengelink R., Brookes M. H., Wall J., 2003, MNRAS, 346, 627
Best P. N., Kauffmann G., Heckman T. M., Brinchmann J., Charlot S., Ivezić Ž., White S. D. M., 2005, MNRAS, 362, 25
Brookes M. H., Best P. N., Rengelink R., Röttgering H. J. A., 2006, MNRAS, 366, 1265
Brookes M. H., Best P. N., Peacock J. A., Röttgering H. J. A., Dunlop J. S., 2007, MNRAS, 385, 1297
Buttiglione S., Capetti A., Celotti A., Axon D. J., Chiaberge M., Macchetto F. D., Sparks W. B., 2009, A&A, 495, 1033
Buttiglione S., Capetti A., Celotti A., Axon D. J., Chiaberge M., Macchetto F. D., Sparks W. B., 2010, A&A, 509, 6
Capetti A., Fanti R., Parma P., 1995, A&A, 300, 643
Casali M. et al., 2007, A&A, 467, 777
Chiaberge M., Capetti A., Celotti A., 2000, A&A, 355, 873
Chiaberge M., Capetti A., Celotti A., 2002, A&A, 394, 791
Ciotti L., Ostriker J. P., 2007, ApJ, 665, 1038
Cohen A. S., Lane W. M., Cotton W. D., Kassim N. E., Lazio T. J. W., Perley R. A., Condon J. J., Erickson W. C., 2007, AJ, 134, 1245
Croom S. M. et al., 2009, MNRAS, 392, 19
Emonts B., Morganti R., Oosterloo T., van Gorkom J., 2008, in Beswick R. J., Diamond P. J., Schilizzi R., eds, Proc. Sci. The Modern Radio Universe: From Planets to Dark Energy, preprint (arXiv:0801.4769)
Evans A. S., Mazzarella J. M., Surace J. A., Frayer D. T., Iwasawa K., Sanders D. B., 2005, ApJS, 159, 197
Fanaroff B. L., Riley J. M., 1974, MNRAS, 167, 31P
Gendre M. A., Wall J. V., 2008, MNRAS, 390, 819
Gendre M. A., Best P. N., Wall J. V., 2010, MNRAS, 404, 1719
Ghisellini G., Celotti A., 2001, MNRAS, 327, 739
Gopal-Krishna, Wiita P. J., 2000, A&A, 363, 507
Hambly N. C., Davenhall A. C., Irwin M. J., MacGillivray H. T., 2001, MNRAS, 326, 1315
Hambly N. C. et al., 2008, MNRAS, 384, 637
Hardcastle M. J., Evans D. A., Croston J. H., 2007, MNRAS, 376, 1849
Herbert P. D., Jarvis M. J., Willott C. J., McLure R. J., Mitchell E., Rawlings S., Hill G. J., Dunlop J. S., 2010, MNRAS, 406, 1841
Hewett P. C., Warren S. J., Leggett S. K., Hodgkin S. T., 2006, MNRAS, 367, 454
Heywood I., Blundell K. M., Rawlings S., 2007, MNRAS, 381, 1093
Ho L. C., Filippenko A. V., Sargent W. L. W., 1995, ApJS, 98, 477
Jackson N., Rawlings S., 1997, MNRAS, 286, 241
Jackson C. A., Wall J. V., 1999, MNRAS, 304, 160
Janssen R. M. J., Röttgering H. J. A., Best P. N., Brinchmann J., 2012, A&A, 541, 62
Kauffmann G. et al., 2003, MNRAS, 346, 1055
Kauffmann G., Heckman T. M., Best P. N., 2008, MNRAS, 384, 953
Ker L. M., Best P. N., Rigby E. E., Röttgering H. J. A., Gendre M. A., 2012, MNRAS, 420, 2644
Kunert-Bajraszewskal M., Labian A., 2010, MNRAS, 408, 2279
Laing R. A., Riley J. M., Longair M. S., 1983, MNRAS, 204, 151
Laing R. A., Jenkins C. R., Wall J. V., Unger S. W., 1994, in Bicknell G. V., Dopita M. A., Quinn P. J., eds, ASP Conf. Ser. Vol. 54, The First Stromlo Symposium: The Physics of Active Galaxies. Astron. Soc. Pac., San Francisco, p. 201
Lawrence A. et al., 2007, MNRAS, 379, 1599
Ledlow M. J., Owen F. N., 1996, AJ, 112, 9
Longair M. S., 1966, MNRAS, 133, 421
Merloni A., Heinz S., 2007, MNRAS, 381, 589
Myers S. T. et al., 2003, MNRAS, 341, 1
Nonino M. et al., 1999, A&AS, 137, 51
Ocaña Flaquer B., Leon S., Combes F., Lim J., 2010, A&A, 518, 9
Owen F. N., Ledlow M. J., 1994, in Bicknell G. V., Dopita M. A., Quinn P. J., eds, ASP Conf. Ser. Vol. 54, The Physics of Active Galaxies. Astron Soc. Pac. San Francisco, p. 319
Prestage R. M., Peacock J. A., 1988, MNRAS, 230, 131
Richards G. T. et al., 2009, ApJS, 180, 67

Rigby E. E., Snellen I. A. G., Best P. N., 2007, MNRAS, 380, 1449
Rigby E. E., Best P. N., Snellen I. A. G., 2008, MNRAS, 385, 310
Shakura N. I., Sunyaev R. A., 1973, A&A, 24, 337
Smolčić V., Riechers D. A., 2012, ApJ, 730, 64
Snellen I. A. G., Best P. N., 2001, MNRAS, 328, 897
Tinti S., de Zotti G., 2006, A&A, 445, 899
Wall J. V., Jackson C. A., 1997, MNRAS, 290, 17
White R. L., 1992, Proc. Astron. Soc. Aust., 10, 140

White R. L. et al., 2000, ApJS, 126, 133
Willott C. J., Rawlings S., Blundell K. M., Lacy M., 2001, MNRAS, 322, 536
Windhorst R. W. et al., 1991, ApJ, 380, 362
Wing J. D., Blanton E. L., 2011, AJ, 141, 88
York D. G. et al., 2000, AJ, 120, 1579
Zirbel E. L., 1997, ApJ, 476, 489
Zirbel E. L., Baum S. A., 1995, ApJ, 448, 521

APPENDIX A: UPDATED DATA IN THE CONFIG CATALOGUE

Table A1. Flux density measurements at 591 MHz from the GMRT data described in Section 2.1.

Source	$S_{591\,\mathrm{MHz}}$ (mJy)	Source	$S_{591\,\mathrm{MHz}}$ (mJy)	Source	$S_{591\,\mathrm{MHz}}$ (mJy)	Source	$S_{591\,\mathrm{MHz}}$ (mJy)	Source	$S_{591\,\mathrm{MHz}}$ (mJy)
C1-128	2434 ± 28	C4-016	113.8 ± 4.6	C4-074	57.3 ± 1.9	C4-116	259.2 ± 4.2	C4-152	25.0 ± 3.4
C1-163	2585 ± 63	C4-019	116.1 ± 1.9	C4-084	79.7 ± 2.6	C4-127	120.0 ± 1.3	C4-158	34.3 ± 2.2
C2-095	1386 ± 19	C4-021	143.0 ± 2.4	C4-088	134.7 ± 3.6	C4-131	68.4 ± 2.0	C4-166	80.1 ± 4.4
C3-219	219.8 ± 1.8	C4-028	115.7 ± 7.0	C4-091	62.3 ± 1.0	C4-132	66.7 ± 2.7	C4-172	119.9 ± 1.7
C4-003	136.3 ± 3.9	C4-040	229.4 ± 2.0	C4-093	118.0 ± 2.3	C4-133	50.0 ± 3.0	C4-176	52.7 ± 5.4
C4-004	117.4 ± 2.7	C4-044	109.2 ± 9.7	C4-097	87.0 ± 1.5	C4-139	81.5 ± 2.7	C4-178	138.7 ± 7.2
C4-006	149.2 ± 3.7	C4-048	135.4 ± 2.5	C4-101	98.7 ± 1.9	C4-140	232.4 ± 2.9	C4-181	210.4 ± 1.6
C4-010	118.0 ± 2.3	C4-052	159.8 ± 2.1	C4-102	98.3 ± 2.0	C4-141	54.8 ± 1.5	C4-183	106.2 ± 1.9
C4-011	813.3 ± 5.9	C4-056	110.1 ± 1.8	C4-103	78.4 ± 1.1	C4-143	52.0 ± 8.3		
C4-014	128.5 ± 4.3	C4-057	113.3 ± 1.6	C4-113	112.6 ± 1.3	C4-144	70.1 ± 2.4		

Table A2. Revised/new spectral index values α, defined as $S_\nu \propto \nu^\alpha$, for sources in the CoNFIG catalogue, computed by: [a]including VLSS flux density data; [b]including CLASS flux density data; [c]including GMRT flux density measurement (as described in Section 2.1); [d]other as described in Section 2.2.

Source	α	Source	α	Source	α	Source	α	Source	α	Source	α
C1-001	-0.27^b	C2-228	-0.81^a	C3-195	-1.04^b	C4-035	-0.84^a	C4-093	-0.60^c	C4-152	1.07^c
C1-002	-0.33^b	C3-002	-0.59^a	C3-201	-0.73^a	C4-040	-0.79^c	C4-097	-0.31^c	C4-153	-0.92^a
C1-076	-0.30^b	C3-006	-0.58^d	C3-206	-0.60^a	C4-041	-0.93^a	C4-098	-0.69^a	C4-157	-0.10^d
C1-138	-0.47^a	C3-010	-0.27^b	C3-216	-0.57^a	C4-044	-0.79^c	C4-101	-0.14^c	C4-158	0.45^c
C1-175	-0.35^d	C3-012	-0.82^a	C3-219	-0.11^c	C4-047	-0.62^d	C4-102	-0.61^c	C4-163	-0.81^a
C1-181	-0.19^d	C3-018	-0.37^b	C3-244	-0.62^a	C4-048	-0.78^c	C4-103	-0.30^c	C4-166	-0.21^c
C1-198	-0.58^b	C3-024	-0.06^b	C3-274	-0.66^a	C4-049	-0.95^a	C4-107	-0.98^a	C4-167	-0.14^d
C1-215	-0.42^{ba}	C3-025	-0.48^a	C3-280	-0.71^a	C4-050	-0.46^d	C4-113	-0.72^c	C4-168	-0.91^a
C1-233	-0.32^{ba}	C3-027	-0.62^a	C3-281	-0.67^a	C4-052	-0.71^c	C4-116	-1.09^c	C4-169	-1.54^b
C1-236	-0.90^b	C3-044	-0.54^a	C3-286	-0.58^b	C4-055	-0.74^d	C4-120	-0.74^a	C4-172	-0.54^c
C1-239	-0.36^{ba}	C3-047	-0.36^b	C4-003	-0.93^c	C4-056	-0.19^c	C4-127	-0.81^c	C4-173	-0.47^d
C2-009	-0.37^b	C3-051	-0.06^b	C4-004	-0.54^c	C4-057	-0.72^c	C4-128	-0.86^a	C4-174	-1.41^b
C2-032	-0.43^b	C3-063	-0.55^a	C4-006	-0.76^c	C4-066	-0.21^b	C4-131	-0.23^c	C4-176	0.09^c
C2-059	-0.44^b	C3-069	-0.72^a	C4-008	-1.00^a	C4-067	-0.71^a	C4-132	-0.15^c	C4-178	-0.38^c
C2-062	-0.27^d	C3-078	-0.45^{ba}	C4-010	-0.62^c	C4-071	-1.53^d	C4-133	0.18^c	C4-180	-0.39^d
C2-102	-0.61^b	C3-079	-0.47^d	C4-011	0.13^c	C4-072	-0.87^a	C4-134	-0.79^a	C4-181	0.03^c
C2-112	-0.23^{ba}	C3-094	-0.77^a	C4-014	0.28^c	C4-074	-0.07^c	C4-135	-0.78^a	C4-183	-0.31^c
C2-155	-0.56^{ba}	C3-116	-1.12^b	C4-015	-0.78^d	C4-078	-0.77^a	C4-139	-0.17^c	C4-184	-0.75^a
C2-161	-0.27^b	C3-123	-0.88^b	C4-016	-0.54^c	C4-080	-0.74^c	C4-140	-0.16^c	C4-185	-0.85^a
C2-162	-0.11^b	C3-137	-1.02^d	C4-019	-0.89^c	C4-082	-0.88^a	C4-141	1.78^c		
C2-165	-0.86^b	C3-139	-0.49^a	C4-021	-1.13^c	C4-084	-0.51^c	C4-142	-0.66^a		
C2-173	-0.82^b	C3-146	-0.63^a	C4-022	-1.17^a	C4-085	-0.24^d	C4-143	0.03^c		
C2-193	-0.18^b	C3-173	-0.51^{ba}	C4-025	-0.50^{ba}	C4-088	-0.81^c	C4-144	-0.31^c		
C2-200	-0.84^d	C3-181	-0.72^a	C4-028	-0.34^c	C4-091	-0.19^c	C4-146	-0.63^{ba}		

Table A3. UKIDSS K-band magnitudes for sources in the CoNFIG catalogue, as defined in Section 2.3, with a 2.0 arcsec aperture diameter. Note that a minimum error of $\Delta K = 0.1$ is assigned. n indicates sources for which this is the first detection of the host-galaxy.

Source	K	Source	K	Source	K	Source	K
C1-011	13.6 ± 0.1	C1-247	15.6 ± 0.1	C3-122	18.1 ± 0.1	C4-073[n]	18.2 ± 0.2
C1-018	14.4 ± 0.1	C1-272	15.3 ± 0.1	C3-127	17.4 ± 0.1	C4-074	16.4 ± 0.1
C1-021	15.7 ± 0.1	C2-010	16.0 ± 0.1	C3-134	15.7 ± 0.1	C4-079[n]	18.0 ± 0.1
C1-036	18.0 ± 0.2	C2-012[n]	18.0 ± 0.1	C3-142	13.4 ± 0.1	C4-080	16.8 ± 0.1
C1-038	15.3 ± 0.1	C2-014	15.9 ± 0.1	C3-144	17.1 ± 0.1	C4-081	17.2 ± 0.1
C1-054	16.8 ± 0.1	C2-019	15.9 ± 0.1	C3-153	17.1 ± 0.1	C4-085	14.4 ± 0.1
C1-055	17.0 ± 0.1	C2-035	17.9 ± 0.1	C3-159[n]	18.5 ± 0.2	C4-086	17.2 ± 0.1
C1-056	12.6 ± 0.1	C2-036	16.2 ± 0.1	C3-166	15.7 ± 0.1	C4-088	17.8 ± 0.1
C1-059	13.4 ± 0.1	C2-038	18.1 ± 0.1	C3-167	15.9 ± 0.1	C4-092	16.2 ± 0.1
C1-066	17.4 ± 0.1	C2-046	16.3 ± 0.1	C3-180	15.0 ± 0.1	C4-093	15.4 ± 0.1
C1-077	15.2 ± 0.1	C2-049	14.6 ± 0.1	C3-189	13.1 ± 0.1	C4-094	16.7 ± 0.1
C1-078	16.7 ± 0.1	C2-052	16.0 ± 0.1	C3-195	13.6 ± 0.1	C4-097[n]	17.9 ± 0.2
C1-082	13.2 ± 0.1	C2-062	15.6 ± 0.1	C3-199[n]	18.1 ± 0.1	C4-098	14.8 ± 0.1
C1-104	16.4 ± 0.1	C2-065	14.8 ± 0.1	C3-208	14.9 ± 0.1	C4-101	17.0 ± 0.1
C1-111	14.8 ± 0.1	C2-069	17.2 ± 0.1	C3-246	17.0 ± 0.1	C4-107	16.5 ± 0.1
C1-121	17.0 ± 0.1	C2-085	17.6 ± 0.1	C3-250[n]	16.6 ± 0.1	C4-111	15.4 ± 0.1
C1-128	13.6 ± 0.1	C2-094	13.7 ± 0.1	C3-253	17.2 ± 0.1	C4-115	15.5 ± 0.1
C1-129	11.6 ± 0.1	C2-103[n]	17.5 ± 0.1	C4-001	17.5 ± 0.1	C4-118	15.9 ± 0.1
C1-133	11.1 ± 0.1	C2-117	15.2 ± 0.1	C4-002	15.8 ± 0.1	C4-119[n]	17.1 ± 0.1
C1-135	10.2 ± 0.1	C2-123	15.6 ± 0.1	C4-003	17.6 ± 0.1	C4-122[n]	17.7 ± 0.1
C1-136	13.5 ± 0.1	C2-126	14.5 ± 0.1	C4-004[n]	18.3 ± 0.2	C4-123	17.9 ± 0.1
C1-144	15.8 ± 0.1	C2-131	17.9 ± 0.1	C4-005[n]	17.7 ± 0.1	C4-125	17.8 ± 0.1
C1-147	17.6 ± 0.1	C2-133	14.9 ± 0.1	C4-007[n]	18.1 ± 0.2	C4-126	17.4 ± 0.1
C1-152	18.3 ± 0.2	C2-153	15.0 ± 0.1	C4-008	18.2 ± 0.2	C4-131	16.9 ± 0.1
C1-153	16.2 ± 0.1	C2-171	16.1 ± 0.1	C4-016	15.6 ± 0.1	C4-137	16.2 ± 0.1
C1-159	15.4 ± 0.1	C2-188	15.7 ± 0.1	C4-020	14.8 ± 0.1	C4-139[n]	18.1 ± 0.2
C1-161	16.0 ± 0.1	C2-191	15.3 ± 0.1	C4-023[n]	18.0 ± 0.1	C4-142	15.8 ± 0.1
C1-168	14.4 ± 0.1	C2-193	16.3 ± 0.1	C4-025	16.4 ± 0.1	C4-145	16.6 ± 0.1
C1-175	14.2 ± 0.1	C2-196	16.4 ± 0.1	C4-027[n]	18.0 ± 0.1	C4-146	14.0 ± 0.1
C1-177	17.2 ± 0.1	C2-204	16.7 ± 0.1	C4-028	15.3 ± 0.1	C4-153	17.5 ± 0.1
C1-178	17.1 ± 0.1	C2-208	16.3 ± 0.1	C4-029	15.4 ± 0.1	C4-155	16.9 ± 0.1
C1-180	17.4 ± 0.1	C2-220	13.8 ± 0.1	C4-035	17.6 ± 0.1	C4-156[n]	17.9 ± 0.1
C1-193	17.8 ± 0.1	C2-233	14.1 ± 0.1	C4-039	17.9 ± 0.1	C4-159	17.2 ± 0.1
C1-194	13.0 ± 0.1	C2-239	14.5 ± 0.1	C4-042	17.5 ± 0.1	C4-161	16.3 ± 0.1
C1-198	15.7 ± 0.1	C3-001	17.7 ± 0.1	C4-043	16.2 ± 0.1	C4-166	14.5 ± 0.1
C1-199	16.0 ± 0.1	C3-006	17.3 ± 0.1	C4-044	14.9 ± 0.1	C4-169	17.8 ± 0.2
C1-204	15.2 ± 0.1	C3-016	16.1 ± 0.1	C4-049	14.2 ± 0.1	C4-170	18.0 ± 0.2
C1-207	15.9 ± 0.1	C3-022	15.5 ± 0.1	C4-050	14.7 ± 0.1	C4-172	16.1 ± 0.1
C1-208	17.3 ± 0.1	C3-047	16.4 ± 0.1	C4-051[n]	18.1 ± 0.2	C4-173	18.4 ± 0.2
C1-211	12.7 ± 0.1	C3-049	16.3 ± 0.1	C4-052	17.3 ± 0.1	C4-174	16.5 ± 0.1
C1-215	17.7 ± 0.1	C3-057	12.3 ± 0.1	C4-054	17.2 ± 0.1	C4-176	15.5 ± 0.1
C1-220	15.9 ± 0.1	C3-060[n]	18.1 ± 0.1	C4-055	14.0 ± 0.1	C4-178	17.2 ± 0.1
C1-225	16.2 ± 0.1	C3-070	18.3 ± 0.2	C4-062	17.1 ± 0.1	C4-179	17.5 ± 0.1
C1-229	14.1 ± 0.1	C3-093	14.6 ± 0.1	C4-064	17.6 ± 0.1	C4-180	16.9 ± 0.1
C1-236	16.6 ± 0.1	C3-097	17.5 ± 0.1	C4-066	17.9 ± 0.1	C4-184	15.1 ± 0.1
C1-238	16.8 ± 0.1	C3-101	17.9 ± 0.1	C4-068[n]	18.2 ± 0.2	C4-188	17.5 ± 0.1
C1-240	18.0 ± 0.1	C3-104	13.4 ± 0.1	C4-071	16.2 ± 0.1		
C1-245	15.4 ± 0.1	C3-105	14.7 ± 0.1	C4-072	16.7 ± 0.1		

Table A4. Coordinates of the 20 new UKIDSS optical identifications for sources in the CoNFIG catalogue, as defined in Section 2.3.

Source	Coordinates (J2000)	Source	Coordinates (J2000)
C2-012	09 36 31.97, +04 22 10.02	C4-027	14 11 10.29, −00 36 01.67
C2-103	11 11 22.64, +03 09 09.67	C4-051	14 15 30.52, +02 23 02.50
C3-060	14 56 28.71, +13 02 40.58	C4-068	14 19 13.52, −00 13 51.21
C3-159	15 18 35.95, +10 32 12.26	C4-073	14 20 34.15, −00 54 59.92
C3-199	15 31 47.96, +10 55 33.20	C4-079	14 23 03.45, +01 39 58.50
C3-250	15 50 11.83, +27 17 59.40	C4-097	14 26 12.95, +02 00 39.38
C4-004	14 08 32.70, −01 31 20.78	C4-119	14 30 00.91, +00 46 26.51
C4-005	14 08 33.36, +01 16 22.05	C4-122	14 30 30.63, +01 01 03.14
C4-007	14 08 46.80, +01 33 56.27	C4-139	14 33 08.85, +00 44 34.90
C4-023	14 10 35.35, −00 41 53.03	C4-156	14 36 30.35, +00 35 19.05

Table A5. Revised redshift for sources in the CoNFIG catalogue.

Source	Redshift	Source	Redshift	Source	Redshift	Source	Redshift
C1-034	$4.5165^{(1)}$	C3-027	$2.2550^{(3)}$	C3-168	$3.2253^{(1)}$	C4-043	$0.4000^{(6)}$
C1-062	$0.8993^{(1)}$	C3-032	$0.2505^{(1)}$	C3-171	$2.1824^{(1)}$	C4-051	$1.6000^{(6)}$
C1-082	$0.3823^{(1)}$	C3-048	$0.3350^{(3)}$	C3-188	$2.7950^{(3)}$	C4-068	$1.8000^{(6)}$
C1-086	$0.5500^{(2)}$	C3-051	$1.2760^{(1)}$	C3-194	$2.2650^{(3)}$	C4-081	$0.8000^{(6)}$
C1-185	$0.2600^{(4)}$	C3-060	$1.6000^{(6)}$	C3-199	$1.6000^{(6)}$	C4-088	$1.3000^{(6)}$
C1-213	$0.5798^{(1)}$	C3-070	$1.8000^{(6)}$	C3-222	$2.5424^{(1)}$	C4-092	$0.4000^{(6)}$
C2-038	$1.6000^{(6)}$	C3-071	$1.6850^{(3)}$	C3-250	$0.6000^{(6)}$	C4-119	$0.8000^{(6)}$
C2-085	$0.6500^{(2)}$	C3-099	$2.2830^{(1)}$	C4-005	$1.2000^{(6)}$	C4-122	$1.2000^{(6)}$
C2-103	$1.1000^{(6)}$	C3-101	$1.5450^{(3)}$	C4-007	$1.6000^{(6)}$	C4-125	$1.3000^{(6)}$
C2-185	$0.6793^{(1)}$	C3-108	$1.8247^{(1)}$	C4-008	$1.7000^{(6)}$	C4-153	$1.0000^{(6)}$
C2-233	$0.3183^{(1)}$	C3-122	$1.6000^{(6)}$	C4-013	$1.6250^{(3)}$	C4-155	$0.2250^{(3)}$
C3-003	$0.9920^{(1)}$	C3-132	$1.6631^{(1)}$	C4-023	$1.5000^{(6)}$	C4-159	$0.9632^{(5)}$
C3-018	$1.5550^{(3)}$	C3-144	$0.8000^{(6)}$	C4-027	$1.5000^{(6)}$	C4-170	$1.4000^{(6)}$
C3-024	$1.0236^{(1)}$	C3-147	$0.5798^{(1)}$	C4-039	$1.4000^{(6)}$		

References: (1) SDSS spectroscopic redshift; (2) Tinti & de Zotti (2006); (3) Richards et al. (2009); (4) White (1992); (5) Croom et al. (2009); (6) UKIDSS K–z relation.

APPENDIX B: CONFIG LOCAL SUB-GROUP

Table B1. Spectral features, richness factor and *I*-band magnitude of local ($z \leq 0.3$) sources in the CoNFIG catalogue. Flux and rest-frame EW of the lines are given in units of Å and 10^{-17} erg cm^{-2} s^{-1} Å^{-1}, respectively. Details of the HEG/LEG classification can be found in Section 3.2. The richness factors are defined in Section 3.3. Column 5 (M) specifies the source morphology. I – FRI; II – FRII; U – Unclassified extended; C – Compact. Column 11 (band) specifies which catalogue and optical band was used to determine the richness factor. *r* – SDSS r magnitude; *R* – SSS R magnitude; *I* – EIS I magnitude. Values of I in Column 12 with an asterisk (∗) were derived from SDSS *i*-band magnitude values. Spectrum reference: 1 – SDSS; 2 – 3CRR emission line catalogue (https://www.astrosci.ca/users/willottc/3crr/3crr.html); 3 – Buttiglione et al. (2009); 4 – Ho, Filippenko & Sargent (1995); 5 – White et al. (2000); 6 – 2dFGRS; 7 – Brookes et al. (2007).

ID	Name	RA	Dec. (J2000)	*M*	[O II]$_{3727\,\text{Å}}$ flux	EW	[O III]$_{5007\,\text{Å}}$ flux	EW	HEG/ LEG	Spec. ref	Richness	Band	I-mag
3C	3C31	01 07 24.95	+32 24 45.15	I					L	2	183.32	*R*	5.75
3C	3C33	01 08 52.86	+13 20 14.36	II					H	2	18.71	*R*	15.71
3C	3C33.1	01 09 44.27	+73 11 57.33	II	45.628	28.507	215.154	263.425	H	3	4.81	*R*	19.31
3C	3C61.1	02 22 35.18	+86 19 06.51	II					H	2	15.97	*R*	19.21
3C	3C66B	02 23 11.41	+42 59 31.51	I					L	2	−263.07	*R*	16.75
3C	3C79	03 10 00.08	+17 05 58.65	II					H	2	−3.97	*R*	17.18
3C	3C83.1B	03 18 15.69	+41 52 27.99	I					L	3	148.39	*R*	11.47
3C	3C84	03 19 48.14	+41 30 42.35	I					L	2	114.53	*R*	6.49
3C	3C98	03 58 54.43	+10 26 02.81	II					H	2	−18.65	*R*	14.65
3C	3C123	04 37 04.37	+29 40 13.86	II					L	2	15.26	*R*	18.32
3C	3C133	05 02 58.50	+25 16 24.00	II					H	2	7.57	*R*	19.47
3C	3C153	06 09 32.53	+48 04 15.35	II					L	2	9.67	*R*	16.54
3C	3C171	06 55 14.73	+54 08 57.39	II					H	2	−41.22	*R*	17.16
3C	3C231	09 55 52.92	+69 40 46.14	I					L	4	−247.57	*R*	7.40
3C	3C382	18 35 03.37	+32 41 46.93	II					H	3	264.15	*R*	14.21

Table B1 – *continued*

ID	Name	RA	Dec.	M	[O II]$_{3727\,Å}$ flux	[O II]$_{3727\,Å}$ EW	[O III]$_{5007\,Å}$ flux	[O III]$_{5007\,Å}$ EW	HEG/ LEG	Spec. ref	Richness	Band	I-mag
		(J2000)											
3C	3C386	18 38 26.22	+17 11 50.16	I					L	3	164.82	R	13.67
3C	3C388	18 44 02.35	+45 33 29.55	II					H	2	73.24	R	14.21
3C	3C390.3	18 42 08.92	+79 46 17.20	II					H	3	10.68	R	15.42
3C	3C401	19 40 25.01	+60 41 36.14	II					L	2	38.79	R	16.60
3C	3C433	21 23 44.55	+25 04 28.04	II					H	2	22.03	R	16.47
3C	3C438	21 55 52.25	+38 00 28.46	II					H	2	51.99	R	17.81
3C	3C452	22 45 48.75	+39 41 15.89	II					H	2	65.29	R	15.38
3C	3C465	23 38 29.39	+27 01 53.53	I					L	2	72.87	R	6.02
C1-003	4C 53.16	07 16 41.09	+53 23 10.30	II							73.24	R	13.29
C1-007	DA 240	07 49 48.10	+55 54 21.00	II					L	1	14.34	R	18.68
C1-008	NGC 2484	07 58 28.60	+37 47 13.80	I	19.609	1.366	18.528	1.638	L	1	29.82	r	12.22
C1-011	3C 192	08 05 31.31	+24 10 21.30	II	121.078	32.772	535.254	58.885	H	1	60.14	r	15.15
C1-015	4C 52.18	08 19 47.55	+52 32 29.50	II							49.28	r	17.79
C1-016	3C 197.1	08 21 33.77	+47 02 35.70	II	0.940	1.363	18.116	9.908	H	1	15.06	r	16.26
C1-017	4C 17.44	08 21 44.02	+17 48 20.50	C	1.504	4.444	4.552	12.601	H	1	−0.00	r	17.58
C1-025	4C 55.16	08 34 54.91	+55 34 21.00	C	65.541	218.714	42.670	125.314	H	1	40.90	r	16.21
C1-026	4C 45.17	08 37 53.51	+44 50 54.60	II	4.688	6.037	88.094	56.810	H	1	−5.46	r	16.44
C1-030	NGC 2656	08 47 53.83	+53 52 36.80	I							39.47	r	15.15
C1-031	4C 31.32	08 47 57.00	+31 48 40.50	II	6.363	1.049	3.764	0.148	L	1	4.77	r	13.28
C1-038	3C 213.1	09 01 05.40	+29 01 45.70	II	14.247	35.530	10.456	14.070	L	1	13.37	r	17.06
C1-046	3C 219	09 21 07.54	+45 38 45.70	II	6.088	6.001	80.084	56.496	H	1	17.20	r	16.16
C1-050	3C 223	09 39 50.20	+35 55 53.10	II	56.397	63.187	441.164	314.377	H	1	28.41	r	16.40
C1-051	3C 223.1	09 41 23.62	+39 44 14.10	II	24.687	9.021	211.159	54.628	H	1	33.17	r	15.30
C1-056	3C 227	09 47 47.27	+07 25 13.80	II	−8.599	2.204	371.339	76.701	H	1	44.76	r	15.95
C1-063	3C 234	10 01 46.73	+28 46 56.50	II	96.280	40.353	1419.283	717.561	H	1	18.41	r	16.14
C1-064	3C 236	10 06 01.74	+34 54 10.40	II	14.244	11.762	22.169	12.268	H	1	10.19	r	15.04
C1-069	4C 39.29	10 17 14.15	+39 01 24.00	II					L	1	85.05	r	18.91*
C1-070	4C 48.29A	10 20 49.61	+48 32 04.20	II	29.706	12.696	7.682	1.425	L	1	−11.25	r	15.63
C1-072	4C 59.13	10 23 38.71	+59 04 49.50	II							−3.23	r	18.93
C1-090	3C 253	11 13 32.13	−02 12 55.20	II							27.98	R	19.31
C1-092	4C 29.41	11 16 34.70	+29 15 20.50	I							61.50	r	13.89
C1-101	4C 61.23	11 37 16.95	+61 20 38.40	II	136.718	96.028	577.092	280.689	H	1	14.88	r	16.16
C1-102	4C 12.42	11 40 27.69	+12 03 07.60	I	13.929	4.485	7.669	1.137	L	1	−21.84	r	14.65
C1-106	4C 37.32	11 44 34.45	+37 10 16.90	II	−3.230	−0.315	26.704	5.616	H	1	17.64	r	15.88
C1-107	3C 264	11 45 05.23	+19 36 37.80	I	46.097	1.626	10.391	0.195	L	1	90.49	r	6.54
C1-114	4C 55.22	11 55 26.63	+54 54 13.60	II	6.559	0.981	0.312	0.002	L	1	−2.25	r	13.66
C1-115	4C 59.17	11 56 03.67	+58 47 05.40	U							2.41	r	18.07
C1-120	4C −04.40	12 04 02.13	−04 22 43.90	II							6.56	R	15.72
C1-128	4C 04.41	12 17 29.83	+03 36 44.00	I	−7.594	−8.168	−0.698	−2.488	L	1	80.10	r	14.43
C1-129	3C 270	12 19 15.33	+05 49 40.40	I			−10.643	−1.581	L	1	57.51	r	10.37
C1-133	M84	12 25 03.78	+12 52 35.20	I			−1.644	−2.737	L	1	93.11	r	8.69*
C1-135	3C 273	12 29 06.41	+02 03 05.10	C					H	3	−11.57	r	11.84*
C1-136	1227+119	12 29 51.84	+11 40 24.20	I	2.589	0.475	−1.233	−3.123	L	1	93.44	r	14.07
C1-137	M87	12 30 49.46	+12 23 21.60	I			0.568	0.001	L	1	132.82	r	9.98
C1-140	4C 16.33	12 36 29.13	+16 32 32.10	I							57.01	r	14.40
C1-144	4C 09.44	12 51 44.47	+08 56 27.80	II							91.09	r	17.84
C1-146	4C 02.34	12 53 03.55	+02 38 22.30	II							16.43	r	17.58*
C1-148	3C 277.3	12 54 11.68	+27 37 32.70	II	−4.707	−5.057	44.959	10.892	H	1	−2.60	r	15.14
C1-155	3C 284	13 11 08.56	+27 27 56.50	II	−35.043	162.162	81.850	77.670	H	1	23.20	r	17.07
C1-157	4C 07.32	13 16 20.51	+07 02 54.30	I							31.79	r	13.07
C1-158	4C 29.47	13 19 06.83	+29 38 33.80	I	12.449	2.925	3.498	0.517	L	1	−17.47	r	14.85
C1-162	3C 285	13 21 21.28	+42 35 15.20	II	9.853	4.198	37.960	15.688	H	1	9.00	r	15.65
C1-163	4C 03.27	13 23 21.04	+03 08 02.80	I	11.860	40.440	48.786	145.240	H	1	−0.51	r	16.83
C1-165	4C 32.44B	13 27 31.71	+31 51 27.30	U							25.90	r	17.17
C1-168	3C 287.1	13 32 56.37	+02 00 46.50	II	26.772	13.199	42.994	30.812	H	1	−3.06	r	16.27*
C1-170	3C 288	13 38 49.67	+38 51 11.10	I	25.085	47.467			L	3	39.26	r	19.46*
C1-172	4C 05.57	13 42 43.57	+05 04 31.50	I	−2.631	−0.301	55.255	13.621	H	1	−10.81	r	15.64
C1-175	4C 12.50	13 47 33.42	+12 17 24.10	C	12.737	20.474	155.231	240.504	H	1	−11.19	r	14.78
C1-176	3C 293	13 52 17.81	+31 26 46.70	I	33.077	18.370	19.589	5.356	L	1	29.15	r	13.52
C1-185	S4 1413+34	14 16 04.18	+34 44 36.50	C							9.07	r	
C1-186	NGC 5532	14 16 53.50	+10 48 40.20	I	23.832	0.543	14.906	0.253	L	1	37.49	r	10.89*

Table B1 – *continued*

ID	Name	RA	Dec.	M	[O II]$_{3727\text{Å}}$		[O III]$_{5007\text{Å}}$		HEG/	Spec.	Richness	Band	I-mag
		(J2000)			flux	EW	flux	EW	LEG	ref			
C1-190	3C 300	14 23 00.81	+19 35 22.80	II					H	1	16.99	r	17.92
C1-194	4C 07.36	14 30 03.34	+07 15 01.30	I	42.137	7.516	16.392	1.025	L	1	−27.35	r	13.49
C1-197	3C 303	14 43 01.45	+52 01 38.20	II	7.362	2.848	218.611	65.857	H	1	24.26	r	19.91*
C1-200	3C 305	14 49 21.74	+63 16 13.90	I	84.726	12.985	313.634	23.957	H	1	106.77	r	13.27
C1-203	B2 1502+28	15 04 19.50	+28 35 34.30	I							56.78	r	15.09
C1-205	3C 310	15 04 58.98	+25 59 49.00	I	32.062	22.572	11.807	2.749	L	1	39.47	r	14.71
C1-209	3C 315	15 13 39.90	+26 07 33.70	I					L	1	−7.66	r	16.30
C1-211	4C 00.56	15 16 40.21	+00 15 02.40	II	30.807	5.221	78.387	19.001	H	1	49.18	r	14.17
C1-216	3C 319	15 24 05.64	+54 28 18.40	II					L	1	23.24	r	17.67
C1-219	3C 321	15 31 50.71	+24 02 43.30	II					H	1	−6.63	r	15.35
C1-226	3C 323.1	15 47 44.23	+20 52 41.00	II	12.246	0.106	283.969	26.345	H	1	17.79	r	15.11
C1-230	3C 326	15 52 26.86	+20 05 01.80	II					L	1	39.58	r	15.99
C1-234	3C 327	16 02 17.21	+01 58 19.40	II					H	1	2.88	R	13.92*
C1-242	NGC 6109	16 17 38.89	+35 00 48.00	I	23.121	2.414	12.021	0.120	L	1	3.51	r	12.77
C1-243	3C 332	16 17 43.28	+32 23 02.40	II	46.467	5.868	179.076	46.312	H	1	−8.99	r	16.06
C1-248	3C 338	16 28 38.34	+39 33 04.70	I					L	1	78.57	r	6.16
C1-258	3C 346	16 43 48.69	+17 15 48.80	I					H	1	44.37	r	15.92
C1-260	4C 39.49	16 53 52.24	+39 45 36.60	C							11.22	r	12.97
C1-261	3C 349	16 59 27.57	+47 03 13.10	II					H	1	27.80	r	19.42*
C1-266	4C 34.47	17 23 20.85	+34 17 57.30	II					H	5	15.37	r	14.94
C1-270	3C 306	14 54 20.30	+16 20 55.80	II	9.610	0.703	−2.929	−1.692	L	1	33.59	r	12.79
C1-271	4C 32.25A	08 31 20.33	+32 18 37.00	II	13.967	3.779	16.312	3.007	L	1	7.28	r	14.14
C1-272	4C 06.32	08 48 41.94	+05 55 35.00	II							63.73	r	17.31
C2-031	4C 21.26	09 54 7.03	+21 22 35.90	II	12.518	4.216	150.113	76.453	H	1	−3.36	r	16.61
C2-041	4C 20.20	10 02 57.12	+19 51 53.50	I	−1.185	−0.339	1.464	0.515	L	1	27.49	r	16.39
C2-045	4C 13.41	10 07 26.10	+12 48 56.21	II	−11.080	−2.362	115.009	3.945	H	1	16.52	r	14.06
C2-049	4C 14.36	10 09 55.50	+14 01 54.10	C	4.908	10.551	4.382	2.530	L	1	10.47	r	16.71
C2-055	4C 41.22	10 15 58.26	+40 46 47.11	II	2.190	0.901	1.058	0.233	L	1	10.24	r	15.81
C2-067	3C 244	10 27 32.89	+48 17 6.40	II	−2.615	15.726	18.087	35.759	H	1	23.67	r	17.85
C2-070	4C 52.22	10 31 43.55	+52 25 37.90	II	4.366	5.374	20.252	13.394	H	1	16.58	r	16.67
C2-102	1108+201	11 11 20.09	+19 55 36.10	C	20.200		10.700		H	3	28.37	r	17.54
C2-105	4C 41.23	11 11 43.62	+40 49 15.30	I	4.393	0.567	1.322	0.062	L	1	58.80	r	14.17
C2-117	4C 05.50	11 24 37.45	+04 56 18.80	II	10.810	76.245	64.728	231.621	H	1	−12.06	r	16.83
C2-118	3C 258	11 24 43.90	+19 19 29.70	C					L	3	−11.53	r	17.95
C2-123	4C 00.40	11 29 35.97	+00 15 17.50	II							30.71	r	17.52*
C2-127	4C 33.27	11 33 9.56	+33 43 12.60	II	−49.036	1440.820	3.835	2.388	L	1	−13.68	r	16.73
C2-134	4C 17.52	11 40 17.03	+17 43 39.00	I			13.402	0.796	L	1	9.06	r	17.26*
C2-141	4C 46.23	11 43 39.63	+46 21 20.70	II	9.633	12.989	4.282	1.999	L	1	56.20	r	15.79
C2-162	1155+251	11 58 25.80	+24 50 17.70	C	10.786	26.324	47.062	91.354	H	1	−9.18	r	16.93
C2-169	4C 58.23	12 02 4.19	+58 02 1.90	I	2.105	0.428	−0.982	−0.910	L	1	67.83	r	15.67*
C2-200	1227+181	12 29 32.62	+17 50 20.90	C							22.16	r	16.93
C2-214	4C 49.25	12 47 7.40	+49 00 18.20	C	6.053	10.609	10.304	9.312	H	1	−5.85	r	17.04
C2-220	1249+035	12 52 22.78	+03 15 50.40	I	4.271	1.144	−1.819	0.002	L	1	−19.98	r	14.68
C2-226	4C 44.22	12 58 1.96	+44 35 20.60	II							30.32	r	17.07
C2-239	4C 08.38	13 15 9.94	+08 41 44.60	II	12.186	7.178	20.918	4.739	L	1	38.92	r	16.13
C3-007	1440+163	14 43 1.74	+16 06 59.90	II							19.81	r	17.13
C3-010	1441+25	14 43 56.94	+25 01 44.50	C							−23.87	r	18.60
C3-015	B1442+195	14 44 34.84	+19 21 33.00	I	0.563	0.076	−1.572	−0.067	L	1	35.81	r	16.50
C3-021	4C 17.60	14 45 57.34	+17 38 30.20	II	8.717	1.066	4.359	0.183	L	1	1.49	r	15.33
C3-029	4C 16.42	14 47 44.55	+16 36 6.00	II							−12.32	r	19.52*
C3-030	1445+149	14 48 4.28	+14 47 4.60	I	−2.085	16.911	−0.667	−2.205	L	1	65.85	r	16.27
C3-032	1446+277	14 48 27.87	+27 33 18.80	C	0.683	2.128	−0.600	−0.769	L	1	47.77	r	17.34
C3-034	3C 304	14 48 50.05	+20 25 34.80	II							5.64	r	17.99
C3-035	1447+213	14 49 19.01	+21 05 48.00	II							8.75	r	17.34
C3-052	1452+258	14 54 22.75	+25 39 55.50	II							0.07	r	18.57*
C3-056	1452+144	14 55 7.32	+14 12 22.20	II							4.73	r	19.40*
C3-057	NGC 5782	14 55 55.36	+11 51 44.70	I	5.401	0.095	−4.513	−0.138	L	1	103.60	r	12.67
C3-058	4C 16.43	14 56 5.65	+16 26 52.80	II	−1.515	7.108	1.387	2.462	L	1	12.13	r	17.24

Table B1 – *continued*

ID	Name	RA	Dec.	M	[O II]$_{3727\,\text{Å}}$ flux	[O II]$_{3727\,\text{Å}}$ EW	[O III]$_{5007\,\text{Å}}$ flux	[O III]$_{5007\,\text{Å}}$ EW	HEG/ LEG	Spec. ref	Richness	Band	I-mag
		(J2000)											
C3-069	4C 28.38	14 57 53.80	+28 32 20.00	II	3.215	3.622	174.347	76.256	H	1	10.94	r	16.32
C3-078	B2 1457+29	14 59 42.07	+29 03 34.10	II							14.08	r	16.51
C3-079	1458+204	15 00 24.05	+20 12 37.80	I							8.60	r	14.84
C3-080	4C 14.57	15 00 21.36	+14 34 59.80	II							−16.15	r	15.48
C3-082	4C 21.44	15 01 28.50	+21 34 20.70	I	1.103	1.946	5.545	0.596	L	1	59.30	r	16.61
C3-089	1500+1832	15 03 1.63	+18 20 32.40	II							11.88	r	18.36
C3-093	MRC1501+104	15 03 39.51	+10 16 2.80	I			19.000		H	1	15.71	r	15.92
C3-104	B1507+105	15 07 21.88	+10 18 46.30	C	59.922	15.452	9.584	1.110	L	1	−5.00	r	14.07
C3-117	J1509+1557	15 09 50.53	+15 57 25.70	C	6.182	6.974	9.215	3.985	L	1	15.11	r	16.32
C3-125	1508+182	15 11 9.08	+18 01 53.80	I	1.246	0.502	0.042	−0.409	L	1	31.78	r	15.42
C3-137	1511+2422	15 13 45.74	+24 11 2.80	II	6.207	3.272	5.773	1.588	L	1	12.60	r	15.39
C3-138	1511+225	15 14 3.55	+22 23 31.50	C							2.04	r	16.96
C3-139	1512+2338	15 14 14.64	+23 27 11.20	II	0.741	0.094	−3.213	−1.644	L	1	−2.88	r	15.18
C3-142	1512+104	15 14 49.50	+10 17 0.90	I	−3.461	−2.461	−5.581	−1.513	L	1	−9.06	r	14.06
C3-146	1513+144	15 16 2.98	+14 18 22.90	II							−28.34	r	17.65
C3-149	1514+215	15 17 4.56	+21 22 42.90	II							3.92	r	18.13
C3-151	1515+176	15 17 24.70	+17 29 28.30	II	5.942	10.378	79.524	98.106	H	1	48.94	r	17.65
C3-165	1519+153	15 21 16.47	+15 12 9.90	U	9.338	37.183	6.619	7.706	L	1	21.39	r	16.82
C3-166	1519+108	15 22 12.15	+10 41 31.00	II							27.23	r	17.22
C3-167	1519+103	15 22 17.09	+10 13 0.50	II							−4.91	r	18.11
C3-172	1521+116	15 23 27.56	+11 30 23.90	I	4.051	4.476	6.282	9.386	H	1	−8.30	r	16.87
C3-173	4C 28.39	15 23 28.40	+28 36 4.10	I	5.511	1.056	1.083	1.006	L	1	9.11	r	14.87
C3-181	1522+130	15 25 8.80	+12 53 18.10	II	2.033	4.946	27.160	34.274	H	1	2.11	r	18.05
C3-189	1525+290	15 27 44.61	+28 55 6.60	I							35.94	r	14.65
C3-190	1525+227	15 27 57.80	+22 33 1.30	II	8.748	0.323	107.179	14.085	H	1	−3.95	r	16.42
C3-195	1528+29	15 30 4.69	+29 00 9.30	II							−35.12	r	14.94
C3-196	1527+234	15 30 5.11	+23 16 22.20	II	0.925	0.071	−3.081	−1.432	L	1	41.16	r	15.19
C3-203	B2 1530+28	15 32 44.30	+28 03 46.40	I	2.405	0.435	−2.623	−1.453	L	1	71.95	r	16.37
C3-208	1531+104	15 34 17.83	+10 17 8.40	I							55.93	r	16.28
C3-209	1532+139	15 34 22.66	+13 49 17.10	II							18.42	r	17.22
C3-211	ARP 220	15 34 57.26	+23 30 11.10	C			14.129	7.417	H	1	−15.41	r	13.23
C3-216	1534+269	15 37 7.76	+26 48 28.50	I							16.65	r	17.66
C3-231	1541+230	15 43 28.53	+22 52 32.80	II	0.190	0.371	1.368	0.178	L	1	29.22	r	15.90*
C3-244	1545+1505	15 47 30.07	+14 56 55.70	I	6.530	1.661	1.756	−0.103	L	1	6.87	r	15.07
C3-266	4C 23.42	15 53 43.61	+23 48 4.70	I	33.605	12.983	42.710	7.505	H	1	4.65	r	15.36
C3-282	4C 10.44	15 56 47.07	+10 37 55.70	I	0.734	0.758	0.913	0.202	L	1	47.93	r	16.14
C3-284	4C 12.56	15 59 6.89	+12 10 26.90	II							2.36	r	18.08
C4-002	1405+026	14 08 28.14	+02 25 48.70	I							0.62	r	17.76
C4-014	1409-0307	14 09 52.02	−03 03 10.30	II	2.693	2.179	2.361	0.684	L	1	54.38	r	15.76
C4-016	1409-0135	14 09 57.00	−01 21 4.70	I							29.73	r	18.12
C4-028	1411+0229	14 11 14.61	+02 17 22.50	U	3.005	0.530	−0.444	−2.266	L	1	6.68	r	17.94
C4-036	NGC 5506	14 13 14.84	−03 12 27.00	I			3335.108	539.967	H	1	−27.96	r	10.84*
C4-044	1414+0182	14 14 9.37	+01 49 10.80	I	−0.404	−1.918	−1.267	−0.164	L	1	12.51	r	16.67
C4-047	LEDA 184576	14 14 57.34	+00 12 17.90	I						6	15.74	r	17.81
C4-049	N274Z243	14 15 11.41	−01 37 2.80	I	0.376	−0.031	0.494	0.156	L	1	26.57	r	15.35
C4-050	N342Z086	14 15 28.72	+01 05 54.20	I					H	6	3.58	r	16.12
C4-055	1416+0219	14 16 13.74	+02 19 22.50	I	4.336	2.100	163.591	58.062	H	1	22.83	r	15.92
C4-056	J141643-02	14 16 43.04	−02 56 11.30	C	0.990	3.815	2.372	1.533	L	1	−5.64	r	16.63
C4-085	N344Z154	14 24 3.40	+00 29 58.70	I	0.199	0.025	−1.419	−0.764	L	1	−1.49	r	15.09
C4-098	N344Z014	14 26 15.51	+00 50 21.70	I	−0.460	0.664	−1.119	−1.316	L	1	15.88	r	15.42
C4-143	1433−0239	14 33 46.69	−02 23 22.50	I							−19.96	r	17.34
C4-146	1434+0158	14 34 10.56	+01 36 46.90	I	0.701	−0.213	−2.508	−1.444	L	1	37.21	r	15.29
C4-150	1432-020	14 34 49.27	−02 15 9.20	II	2.694	3.408	0.820	0.091	L	1	39.54	r	17.53
C4-155	1436+0181	14 36 9.04	+01 48 49.20	C							29.71	r	19.86*
C4-166	1437−0025	14 37 42.80	−00 15 4.20	I	0.737	0.266	−3.489	−0.288	L	1	61.25	r	15.50
C4-176	1438−0133	14 38 20.57	−01 20 6.60	II							−13.49	r	17.53
C4-178	1438−0100	14 38 25.93	−01 00 1.50	I					L	6	30.49	r	19.65*
C4-184	1438+0068	14 38 48.87	+00 40 59.20	I	18.829	29.574	18.254	16.191	H	7	7.21	r	16.14*
CE-008	CE-008	09 57 30.07	−21 30 59.80	II					L	7	48.94	I	17.77
CE-009	CE-009	09 49 35.43	−21 56 23.50	C					H	7	21.24	I	18.28
CE-018	CE-018	09 55 13.60	−21 23 3.10	C					H	7	40.64	I	14.88

Table B1 – *continued*

ID	Name	RA	Dec.	M	[O II]$_{3727\,\text{Å}}$		[O III]$_{5007\,\text{Å}}$		HEG/	Spec.	Richness	Band	I-mag
		(J2000)			flux	EW	flux	EW	LEG	ref			
CE-030	CE-030	09 45 55.86	−20 28 30.20	I					L	7	99.51	*I*	16.41
CE-041	CE-041	09 49 18.18	−20 54 45.40	I					L	7	8.65	*I*	17.10
CE-075	CE-075	09 45 26.97	−20 33 55.00	II					L	7	77.71	*I*	16.73
CE-076	CE-076	09 57 45.89	−21 23 23.60	C					L	7	25.05	*I*	17.23
CE-084	CE-084	09 55 45.19	−21 25 23.00	II					H	7	−0.91	*I*	15.11
CE-093	CE-093	09 46 18.86	−20 37 57.40	I					L	7	10.25	*I*	17.41
CE-095	CE-095	09 54 21.48	−21 48 7.20	U					H	7	153.05	*I*	16.92
CE-108	CE-108	09 56 49.76	−20 35 25.90	C					L	7	−13.43	*I*	17.09
CE-110	CE-110	09 55 11.49	−20 30 18.70	I					L	7	20.82	*I*	17.52
CE-121	CE-121	09 52 1.20	−20 24 56.50	C					H	7	−17.36	*I*	17.15
CE-122	CE-122	09 56 37.11	−20 19 5.50	II					L	7	22.47	*I*	16.94

This paper has been typeset from a TEX/LATEX file prepared by the author.